SYNTHESIS AND CHARACTERIZATION OF COPPER BASED
BULK AMORPHOUS ALLOYS

A THESIS SUBMITTED TO
THE GRADUATE SCHOOL OF NATURAL AND APPLIED SCIENCES
OF
MIDDLE EAST TECHNICAL UNIVERSITY

BY

ERDEM MERMER

IN PARTIAL FULFILLMENT OF THE REQUIREMENTS
FOR
THE DEGREE OF MASTER OF SCIENCE
IN
METALLURGICAL AND MATERIALS ENGINEERING

July 2013

Approval of the thesis:

SYNTHESIS AND CHARACTERIZATION OF COPPER BASED BULK AMORPHOUS ALLOYS

Submitted by **ERDEM MERMER** in partial fulfillment of the requirements for the degree of **Master of Science in Metallurgical and Materials Engineering Department, Middle East Technical University** by

Prof Dr. Canan ÖZGEN
Dean, GraduateSchool of **Natural and Applied Sciences**   ⎯⎯⎯⎯⎯

Prof. Dr. C. Hakan GÜR
Head of Department, **Metallurgical and Materials Engineering**   ⎯⎯⎯⎯⎯

Prof. Dr. M. Vedat AKDENİZ
Supervisor, **Metallurgical and Materials Engineering Dept., METU**   ⎯⎯⎯⎯⎯

Prof. Dr. Amdulla O. MEKHRABOV
Co-Supervisor, **Metallurgical and Materials Engineering Dept., METU** ⎯⎯⎯⎯⎯

Examining Committee Members:

Prof. Dr. Rıza GÜRBÜZ
Metallurgical and Materials Eng. Dept., METU   ⎯⎯⎯⎯⎯

Prof. Dr. C. M. Vedat AKDENİZ
Metallurgical and Materials Eng. Dept., METU   ⎯⎯⎯⎯⎯

Prof. Dr. Amdulla O. MEKHRABOV
Metallurgical and Materials Eng. Dept., METU   ⎯⎯⎯⎯⎯

Assoc.Prof. Dr. Arcan DERİCİOĞLU
Metallurgical and Materials Eng. Dept., METU   ⎯⎯⎯⎯⎯

Assist. Prof. Dr. İlkay KALAY
Materials Science and Eng. Dept., Çankaya University   ⎯⎯⎯⎯⎯

Date: 16.07.2013

I hereby declare that all information in this document has been obtained and presented in accordance with academic rules and ethical conduct. I also declare that, as required by these rules and conduct, I have fully cited and referenced all material and results that are not original to this work.

Name, Last name: Erdem MERMER

Signature:

ABSTRACT

SYNTHESIS AND CHARACTERIZATION OF COPPER BASED BULK AMORPHOUS ALLOYS

MERMER, Erdem
M.S., Department of Metallurgical and Materials Engineering
Supervisor: Prof. Dr. M. Vedat AKDENİZ
Co-Supervisor: Prof. Dr. Amdulla O. MEKHRABOV

June 2013, 59 Pages

Copper based bulk metallic glasses (BMG's) are one of the promising advanced materials due to their unique mechanical properties, high glass forming ability (GFA) and low cost. In this thesis, the aim is to synthesize Cu-Hf based BMG's and to investigate the crystallization behavior. Moreover, the crystallization kinetics by means of activation energies, critical cooling rate, nanocrystallization and Avrami exponents have been studied.

$Cu_{70}Hf_{30}$ and $Cu_{50}Hf_{50}$ binary alloys were produced via arc melting with suction casting unit. However, amorphous structure could not be achieved because of the necessity of lower free energy arose from higher entropy. Therefore, aluminum was added to Cu-Hf system to stabilize the melt and to increase GFA which allowed producing amorphous samples. Thermal analysis studies showed that GFA parameters such as T_{rg}, ΔT_x are in good agreement with the results reported in the literature.

It was observed that $Cu_{49}Hf_{42}Al_9$ ternary alloy solidifies through eutectic reaction at 910 ºC under near equilibrium conditions. However, it was shown that suppression of this eutectic reaction under non-equilibrium cooling conditions lead to the formation of an amorphous phase. The critical cooling rate required for the suppression of the eutectic reaction was determined as 1.25 K/s by isochronal crystallization kinetics. Annealing of these amorphous samples at temperatures around T_x lead to single stage crystallization of $CuHf_2$ nanocrystals with an average size of about 20 nm. The average Avrami exponent value was estimated to be 2.3 implying the crystallization process was governed by diffusion controlled three-dimensional growth with decreasing nucleation rate.

Keywords: Bulk metallic glasses, Cu-Hf system, Suction casting, Crystallization Kinetics

ÖZ

BAKIR ESASLI İRİ VE HACİMLİ CAMSI ALAŞIMLARIN ÜRETİMİ VE KARAKTERİZASYONU

MERMER, Erdem
Yüksek Lisans, Metalurji ve Malzeme Mühendisliği Bölümü
Tez Yöneticisi: Prof. Dr. M. Vedat AKDENİZ
Ortak Tez Yöneticisi: Prof. Dr. Amdulla O. MEKHRABOV

Temmuz 2013, 59 Sayfa

Bakır bazlı iri ve hacimli metalik camlar; kendilerine özgü mekanik özellikleri, yüksek cam oluşturma kabiliyetleri ve düşük maliyetleri nedeniyle gelecek vaadeden gelişmiş malzemelerden biridir. Bu tezde amaç, Cu-Hf bazlı iri ve hacimli metalik camları sentezlemek ve bu alaşımların kristallenme davranışını araştırmaktır. Ayrıca; aktivasyon enerjileri, kritik soğutma hızı, nanokristallenme ve Avrami üslerinin incelenmesi vasıtasıyla kristallenme kinetiği çalışılmıştır.

$Cu_{70}Hf_{30}$ ve $Cu_{50}Hf_{50}$ ikili alaşımları emme döküm ünitesi olan ark eritme sistemiyle üretilmiştir. Buna rağmen, amorf yapı elde edilememiştir. Bunun nedeni; yüksek entropiden dolayı oluşan düşük serbest enerji gerekliliğidir. Bu yüzden dolayı, eriyiği stabilize edip cam oluşturma kabiliyetini arttırmak amacıyla Cu-Hf sistemine Aluminyum eklenmiştir. Böylece, amorf numuneler üretilebilmiştir. Bu numuneler üzerine yapılan termal analiz çalışmaları, T_{rg} ve ΔT_x gibi cam oluşturma kabiliyeti parametrelerinin literatürde bildirilen sonuçlarla iyi bir uyum içerisinde olduğunu göstermiştir.

$Cu_{49}Hf_{42}Al_9$ üçlü alaşımının, dengeye yakın soğutma koşulları altında 910 °C de ötektik katılaştığı gözlemlenmiştir. Bununla birlikte denge dışı soğutma koşulları altında bu ötektik reaksiyonun bastırılmasının amorf bir faz oluşumuna yol açtığı gösterilmiştir. Ötektik reaksiyon bastırılması için gerekli olan kritik soğutma hızı eş zaman kristallenme kinetiği ile 1.25 K/s olarak belirlenmiştir. Amorf numunelerin kristallenme sıcaklığı etrafındaki sıcaklıklarda tavlanmaları, ortalama 20 nm boyutunda tek aşamada kristallenen $CuHf_2$ fazının oluşmasını sağlamıştır. Ortalama Avrami üs değeri 2,3 olan bu kristallenme prosesi, çekirdeklenme hızı azalan difüzyon kontröllü üç boyutlu büyüme ile gerçekleşmiştir.

Anahtar Kelimeler: İri ve hacimli metalik camlar, Cu-Hf sistemi, Emme döküm, Kristallenme Kinetiği

To my parents;

Selma-Tekin Mermer

and brother;

Erdinç Mermer

and İpek…

ACKNOWLEDGEMENTS

TABLE OF CONTENTS

LIST OF TABLES

TABLES

LIST OF FIGURES

FIGURES

CHAPTER 1

INTRODUCTION

Because their technology future promises, bulk vitreous alloys have been studied for twenty years [1]. They have outstanding properties compared to their crystalline parts. The superior properties arise from the random arrangement of atoms of amorphous alloys [2].

Metallic glasses are usually synthesized from the liquid state of the alloy by using rapid solidification techniques. The main point to obtain vitreous phase is undercooling. Thus, if a cooling rate is reached a critical value, development of crystalline phases can be avoided [3].

Since the first discovery of metallic glasses, both ferrous and non-ferrous alloy systems were studied. Among them, Cu-based alloys are very popular due to their advantages. Some of the remarkable advantages of the Cu-based alloys are that they have low cost [4], high ductility with high strength [5] and high glass forming ability [6].

In this thesis, the aim is to synthesize Cu-Hf based bulk metallic glasses, characterize and study about crystallization kinetics. Initially, there have been attempts on Cu-Hf binary alloys in order to obtain amorphous structure. $Cu_{70}Hf_{30}$ and $Cu_{50}Hf_{50}$ binary compositions were chosen on the either side of the congruent point due to promising solidification sequences. $Cu_{49}Hf_{42}Al_9$ alloy was selected for a detailed survey on solidification behavior and crystallization kinetics due to its high glass forming ability [7]. Many studies and experiments were done about glass forming ability and mechanical properties; however, the crystallization kinetics of this alloy has not been specifically searched. For this reason, this study includes crystallization kinetics and thermal stability experiments in addition to the nanocrystallization. These studies might be a key for the application of $Cu_{49}Hf_{42}Al_9$ alloy in the future.

The literature review of this study and concepts about glass formation are presented in chapter two. Experimental procedure details are shown in chapter three. Experimental results and discussion are given in chapter four. Conclusions begin in chapter five.

CHAPTER 2

LITERATURE REVIEW

2.1 HISTORY OF METALLIC GLASSES

The product history of metallic glasses began with the formation of $Au_{75}Si_{25}$ alloy in 1960, by Duwez. They produced this alloy by using rapid cooling technique which is a splat-quenching method. The cooling rate was so high (10^6 Ks^{-1}) that the dimensions of metallic glass were very small in shape and size [8]. Chen et al. [9] reported some Pd based metallic glasses with 1 mm diameter in 1969. The cooling rate of these glasses was 10^3 Ks^{-1}.

In 1984, Turnbull et al. [10] produced $Pd_{40}Ni_{40}P_{20}$ vitreous alloy. They used flux melting technique to eliminate heterogeneities. The cooling rate was under 10 Ks^{-1} and the diameter was 1 cm. It is generally accepted that this glass is the first bulk metallic glass.

In the late 1980's and early 1990's, Inoue's group studied on some other glass forming alloy systems based on La-Al-Ni and La-Al-Cu [11]. They acquired the amorphous alloys under cooling rate of 100 Ks^{-1} and the products were in diameter of several centimeters [12].

Peker and Johnson [13] succeed in development of well-known $Zr_{41.2}Ti_{13.8}Cu_{12.5}Ni_{10}Be_{22.5}$ bulk metallic glass in 1993. The glass was produced with the cooling rate of 1 Ks^{-1} and the supercooled liquid region extended to above 100 K. Figure 2.1 displays the development of casting thickness of metallic glasses up to 2000's. The systems examined so far are based on Zr, Fe, Ni, Ti, Cu and rare-earth based elements. Some ferrous and non-ferrous bulk glass forming systems are demonstrated in Table 2.1.
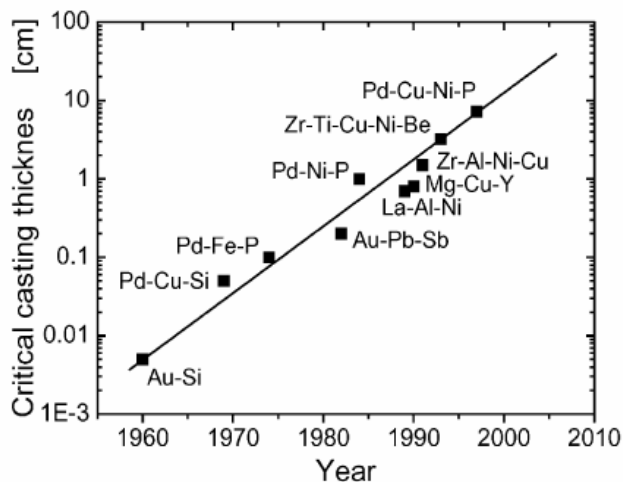
Figure 2.1 The critical casting thickness with the development of metallic glasses [14].

Table 2.1 Bulk metallic glasses reported up to 2010 [15]

1. Non-ferromagnetic alloy systems	Year	2. Ferromagnetic alloy systems	Year
Mg-Ln-M (Ln=lanthanide metal, M=Ni,Cu,Zn)	1988	Fe-(Al-Ga)-(P,C,B,Si,Ge)	1995
Ln-Al-TM (TM=Fe,Co,Ni,Cu)	1989	Fe-(Nb,Mo)-(Al,Ga)-(P,B,Si)	1995
Ln-Ga-TM	1989	Co-(Al,Ga)-(P,B,Si)	1996
Zr-Al-TM	1990	Fe-(Zr,Hf,Nb)-B	1996
Zr-Ln-Al-TM	1992	Co-(Zr,Hf,Nb)-B	1996
Ti-Zr-TM	1993	Fe-Co-Ln-B	1998
Zr-Ti-TM-Be	1993	Fe-Ga-(Cr,Mo)-(P,C,B)	1999
Zr-(Ti,Nb,Pd)-Al-TM	1995	Fe-(Cr,Mo)-(C,B)	1999
Pd-Cu-Ni-P	1996	Ni-(Nb,Cr,Mo)-(P,B)	1999
Pd-Ni-Fe-P	1996	Co-Ta-B	1999
Ti-Ni-Cu-Sn	1998	Fe-Ga-(P,B)	2000
Ca-Cu-Ag-Mg	2000	Ni-Zr-Ti-Sn-Ti	2001
Cu-Zr,Cu-Hf	2001	Ni-(Nb,Ta)-Zr-Ti	2002
Cu-(Zr,Hf)-Ti	2001	Fe-Si-B-Nb	2002
Cu-(Zr,Hf)-Al	2003	Co-Fe-Si-B-Nb	2002
Cu-(Zr,Hf)-Al-(Ag,Pd)	2004	Ni-Nb-Sn	2003
Pt-Cu-Ni-P	2004	Co-Fe-Ta-B-Si	2003
Ti-Cu-(Zr,Hf)-(Co,Ni)	2004	Ni-Pd-P	2004
Au-Ag-Pd-Cu-Si	2005	Fe-(Cr,Mo)-(C,B)-Ln (Ln=Y,Er,Tm)	2004
Ce-Cu-Al-Si-Fe	2005	Co-(Cr,Mo)-(C,B)-Ln (Ln=Y,Tm)	2005
Cu-(Zr,Hf)-Ag	2005	Ni-(Nb,Ta)-Ti-Zr-Pd	2006
Pd-Pt-Cu-P	2007	Ni-Pd-P-B	2009
Zr-Cu-Al-Ag-Pd	2007	Fe-(Nb,Cr)-(P,B,Si)	2010
Ti-Zr-Cu-Pd	2007		
Ti-Zr-Cu-Pd-Sn	2007		

2.2 GLASS FORMATION

Glass formation of metallic alloys could be possible when crystallization is prevented. Thermodynamics and kinetics influence the glass forming ability of metallic alloys.

2.2.1 Thermodynamics of Glass formation

The entropy of liquid is higher than the crystalline solid, i.e, the liquid has more random arrangement at the melting temperature. Upon undercooling, the entropy difference between liquid and crystal decreases [16]. This situation continues until a temperature comes out. Under that temperature, the entropy of liquid becomes lower than the crystal. Kauzmann [17] specified the temperature, T_k, as the glass transition temperature which is shown on the Figure 2.2.
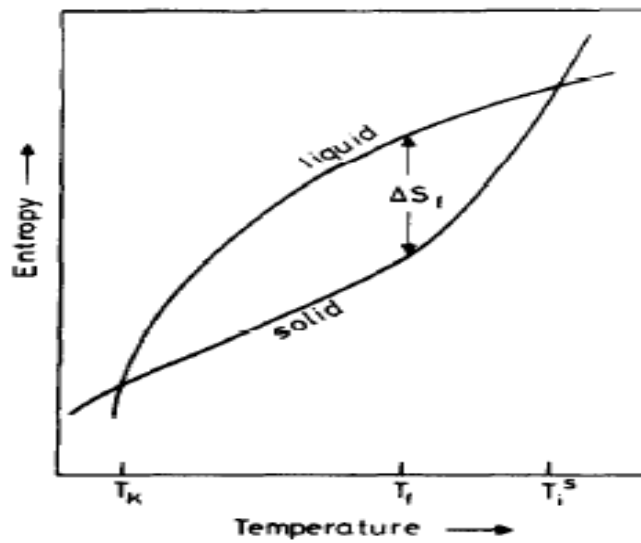
Figure 2.2 Schematic entropy-temperature phase diagram showing Kauzmann temperature, T_k [17]

Turnbull [18] defined a formulation about the free energy difference between the solid and undercooled liquid. The equation is;

$$\Delta G = \Delta H - T\Delta S \tag{2.1}$$

where
$$\Delta H = \Delta H_f - \int_T^{T_f} \Delta C_p dT \tag{2.1a}$$

and
$$\Delta S = \Delta S_f - \int_T^{T_f} \frac{\Delta C_p}{T} dT \tag{2.1b}$$

where ΔH_f is the enthalpy and ΔS_f is the entropy, T_f is the temperature of fusion and ΔCp is the difference of heat stability between an undercooled liquid and solid at a temperature, T. Multicomponent systems cause high entropy difference. Low chemical potential decreases the free energy into a stable temperature due to low enthalpy and the high liquid/solid interfacial energy. Thermodynamic factors show that random packing increase with an

5

increasing ΔS_f which is also effective in decreasing ΔH_f and increasing solid/liquid interfacial energy in multiple alloy systems. Therefore, a high GFA is acquired [19].

2.2.2 Kinetics of Glass formation

Crystallization kinetics study is a necessity to understand the GFA of an amorphous alloy. Some parameters are taken into account when kinetic aspects are examined. The most important one is viscosity. Some methods are used to calculate viscosity from the equilibrium state of undercooled liquid near T_g [20-22]. The viscosity η can be found by Vogel-Fulcher-Tammann equation [23]:

$$\eta = \eta_0 \, exp \left(\frac{DT_0}{T - T_0} \right) \tag{2.2}$$

Viscosity alterations of a liquid are applied to classify different liquids since viscosity indicates the atomic movement of a liquid when it is supercooled. Figure 2.3 shows some viscosity measurements of some glass forming materials. SiO_2 is the best glass forming material which has low VFT temperature and a very high melt viscosity. On the contrary, D-terphenly is fragile because its fragility value is 5 and has low melt viscosity. The melt viscosity of bulk metallic glasses are between 2-5 Pa and fragility value is 20. These features indicate that bulk metallic glasses can be classified as strong glasses [22].
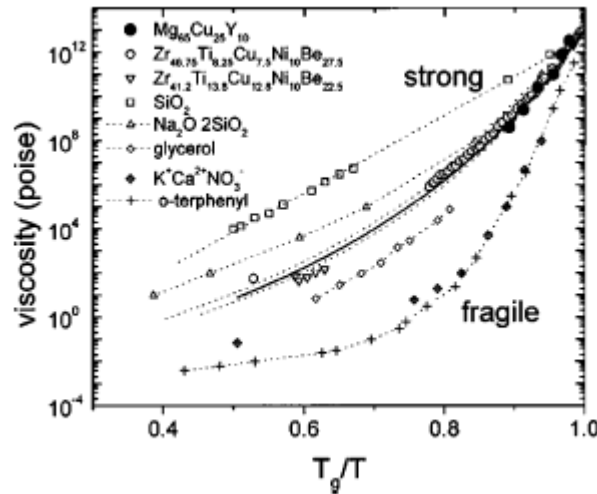
Figure 2.3 Viscosity values of some glass forming materials [24]

2.3 GLASS FORMING ABILITY

Glass-forming ability (GFA) is an easiness to vitrify the liquid on cooling. Comprehension of glass forming ability of materials is significant in order to produce more bulk glass forming alloy systems. For this reason, both experimentally and theoretically theories were suggested by many researches.

Inoue et al. [15] defined three criteria about glass forming ability after evaluating the experimental results of bulk vitreous alloys. The criterion are that (1) the alloys should have

more than three or more elements, (2) the atomic size mismatch is required to be above 12% among the main constituent elements, (3) negative enthalpy of mixing between the main three elements is essential.

2.3.1 Parameters Used in Evaluating of Glass Forming Ability

Other way of assessing glass forming ability is to evaluate some specific temperatures. These temperatures are mainly obtained from differential scanning calorimetry studies. A typical DSC curve is given on the Figure 2.4.
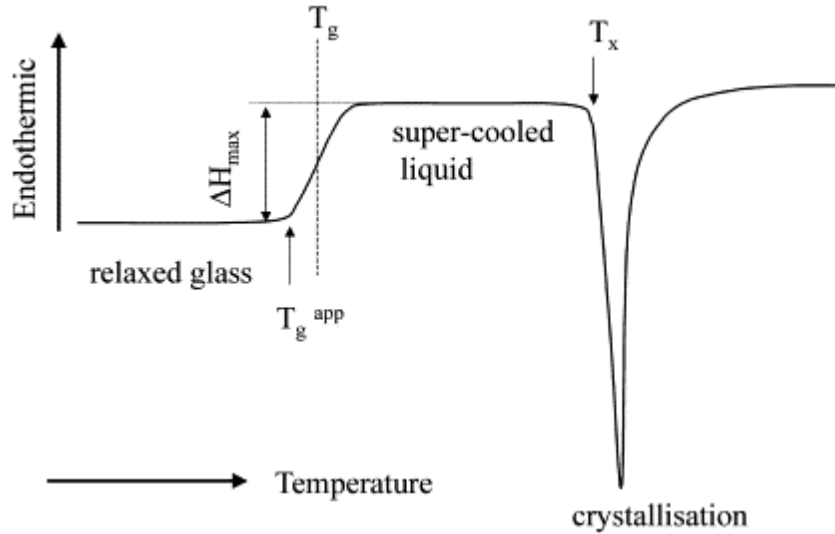
Figure 2.4 A schematical DSC curve of heating [25]

Turnbull [26] proposed a dimensionless parameter which is called reduced glass transition temperature (T_{rg}), showing the ratio of glass transition temperature (T_g) to liquidus temperature (T_l). Inoue et al [27] suggested that extention supercooled liquid region is a good indicator of glass forming ability and defined it as ΔT_x ($=T_x-T_g$) where T_x is the onset of crystallization temperature.

It is generally believed that larger ΔT_x and T_{rg} in the range of 0,66-0,69 indicates higher GFA [28].

Mondal and Murty [29] defined α and β parameter s. They stated that T_l is an estimation of stability of the liquid and T_x is an indicator of thermal stability of bulk metallic glass. By taking these into consideration, α parameter was defined as;

$$\alpha = \frac{T_x}{T_l} \qquad (2.3)$$

Then, they represent β parameter as glass forming ability measurement. The β parameter was shown as;

$$\beta = \frac{T_x}{T_g} + \frac{T_g}{T_l} \qquad (2.4)$$

7

As a result of absence of T_g of some bulk metallic glass systems on heating, they assumed that $T_g = T_x$ and restructured the equation as;

$$\beta = 1 + \frac{T_x}{T_l} \qquad (2.5)$$
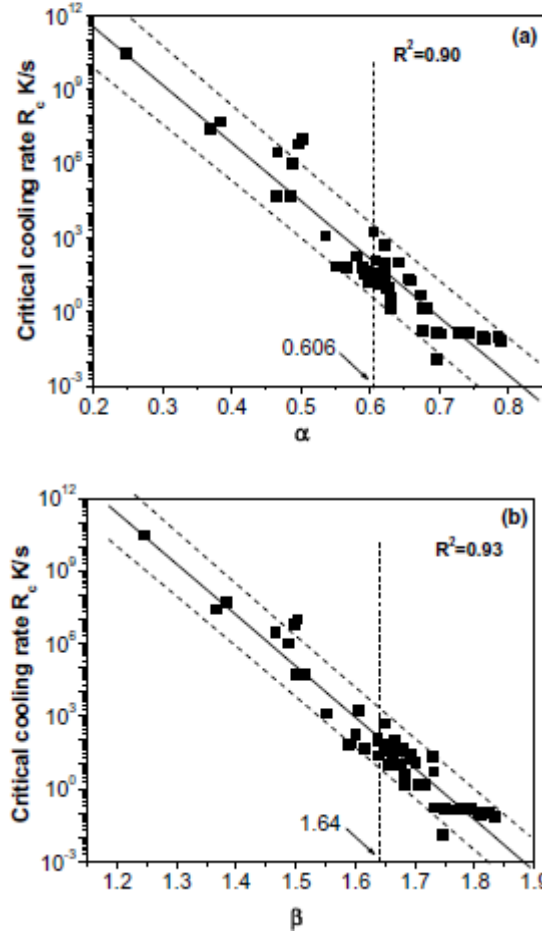
Figure 2.5 Correlation between R_c and α and β [29]

FAN et al. [30]) described a dimensionless parameter Φ with considering the fragility concept and nucleation theory.

$$\Phi = T_{rg} \left(\frac{\Delta T_x}{T_g} \right) {}^{\wedge} \alpha \qquad (2.6)$$

where α is a constant. They evaluated that Φ parameter is in a good agreement with critical cooling rate.

Another parameter is established by Hruby [31] such as;

$$K_{gl} = \frac{T_x - T_g}{T_m - T_x} \qquad (2.7)$$

2.3.2 Considerations Based on Phase Diagrams

Akdeniz et.al [32] examined the solidification behavior of both ferrous and non-ferrous bulk glass forming systems. They examined the systems in near equilibrium and in rapid cooling conditions to associate the glass forming ability and type or nature of invariant reactions. According to their observations, the system entering the order of peritectic and eutectic reactions with high enthalpy ratio is believed to have high glass forming ability. They also defined that suppression of eutectic reaction during solidification bring forth to amorphous structure. Their schematical phase diagram and thermal pattern are given on the Figure 2.6.
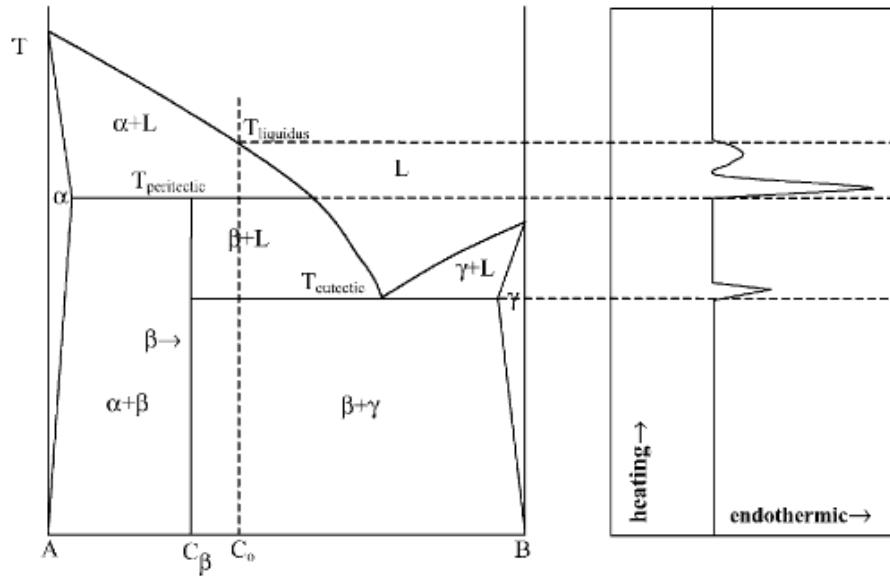
Figure 2.6 Schematical Phase diagram and thermal pattern of a binary alloy having melting sequence of peritectic and eutectic reactions [32]

According to many researches, eutectic compositions are favorable for glass formation of metallic alloys. The reasons are that the eutectic point is the lowest point of the liquid phase in the phase diagram. At this composition, the temperature interval between the crystallization and glass transition is low. For this reason, the time for crystallization is decreased. Thus, the liquid is more stable than the crystalline phases which make glass formation easier [33]. Zhao et al. [34] produced $Ti_{43.89}Cu_{43.60}Zr_{6.75}Ni_{5.76}$ bulk metallic glass based on the above idea. They determined the alloy compositions according to the deep eutectic compositions of Ti-Cu, Ti-Ni, Cu-Zr, Ni-Zr binary phase diagrams.

2.4 Cu-BASED BULK METALLIC GLASSES

The first Cu-rich bulk metallic glass synthesized by Lin et al. [35] in 1995. The alloy composition was $Cu_{47}Ti_{34}Zr_{11}Ni_8$ and cast into 4 mm thickness. Yim et al. [36] developed the glass forming ability of Cu-Ti-Zr-Ni by adding Si element which enhanced the thickness of the alloy to 7 mm. Inoue et al. fabricated Cu-based $Cu_{60}Zr_{30}Ti_{10}$ [37] and $Cu_{60}Hf_{25}Ti_{15}$ [38] amorphous alloys with 4 mm diameter by copper mold casting.

Some researches tried to develop Cu-based bulk metallic glasses with binary compositions. In 2004, Wang et al. [39] studied Cu-Zr binary system considering eutectic compositions.

They, firstly choosed $Cu_{61.8}Zr_{38.2}$ eutectic composition but bulk metallic glass could not be obtained. $Cu_{64.5}Zr_{35.5}$ bulk metallic glass was synthesized with 2 mm diameter by decreasing Zr content.

Duan et al. [40] worked on Cu-Hf binary system in 2005. They produced amorphous samples 0.5 m to 2mm diameter. The highest glass forming ability was found at 66 at.%Cu-34 at.% Hf composition. T_g value was 784 K and T_{rg} was 0.62. They also investigated the mechanical properties of the binary glass forming alloy. The alloy exhibited 2.1 GPa fracture strength and 1.8 % percent total strain.

Jia et al. [41] discovered $Cu_{49}Hf_{42}Al_9$ vitreous alloy by copper mold casting. The diameter of the bulk metallic glass was 10 mm. The alloy had large supercooled region as 85 K. Thermal datas of the $Cu_{49}Hf_{42}Al_9$alloy are illustrated in the Table 2.2.

Table 2.2 Thermal datas of the $Cu_{49}Hf_{42}Al_9$ alloy [41]

Diameter of as-cast rods(mm)	T_g (K)	T_x (K)	ΔT_x (K)	ΔH_x (kJ/mol)	T_m (K)	T_l (K)	T_{rg}
1	777	863	86	4.16	-	-	-
10	778	863	85	4.12	1212	1249	0.622

They made a research on the mechanical properties. They stated that the alloy presented 10.5-13 % plastic strain and 2620 MPa fracture stress. The high plasticity was explained with the formation of shear bands in compression test. The compressive-strain curve and SEM view of $Cu_{49}Hf_{42}Al_9$ alloy are shown on the Figure 2.7.
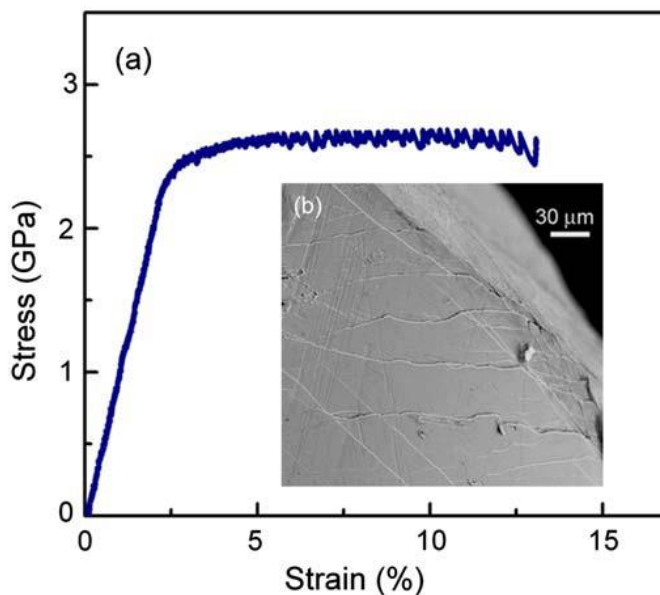
Figure 2.7 a) compressive stress-strain curve b) SEM foto of the fractured sample of $Cu_{49}Hf_{42}Al_9$ alloy [41].

Same group [42] surveyed compositional dependence of the Cu-Hf-Al ternary alloys. They had attemps on different compositions and obtained valuable information about Cu-Hf-Al ternary alloys. The critical thickness, thermal datas of the dissimilar compositions are shown in the Table 2.3.

Table 2.3 Critical casting diameters and thermal properties of different Cu-Hf-Al based bulk metallic glasses[42]

Alloy	Composition	D_c(mm)	T_g(K)	T_x(K)	ΔT_x(K)	ΔH_x(kJ/mol)	T_{rg}
A	$Cu_{53}Hf_{42}Al_5$	1.5	770	865	95	5.78	0.613
B	$Cu_{51}Hf_{42}Al_7$	3	776	825	49	5.17	0.622
C	$Cu_{49}Hf_{42}Al_9$	10	780	863	83	4.12	0.615
D	$Cu_{47}Hf_{42}Al_{11}$	3	783	839	56	3.26	0.608
E	$Cu_{54}Hf_{39}Al_7$	3	776	832	56	4.73	0.615
F	$Cu_{53}Hf_{40}Al_7$	6	777	860	83	5.45	0.623
G	$Cu_{52}Hf_{41}Al_7$	3	776	827	51	5.08	0.622
H	$Cu_{50}Hf_{43}Al_7$	3	776	824	48	5.41	0.616
I	$Cu_{49}Hf_{44}Al_7$	4	773	825	52	6.02	0.601
J	$Cu_{48}Hf_{45}Al_7$	3	773	827	54	6.54	0.579

They also analyzed $Cu_{49}Hf_{42}Al_9$ alloy from the kinetic point of view. The fragility parameter D^* was estimated to be 16.8 which is reasonable value of high glass forming ability. Other approach of Jia et al. is about the solidification microstructures [42]. They indicated that $Cu_{49}Hf_{42}Al_9$ alloy goes eutectic reaction before the glass formation. The eutectic structure is composed of $(L \rightarrow Cu_{10}Hf_7 + CuHf_2 + CuHfAl)$. Al addition was stabilized the Cu-Hf binary alloy and eutectic reaction temperature dropped 47 K resulting in high glass forming ability.

Zhang et al [43] employed quaternary Cu-Zr-Ag-Al alloys. The production technique was injection mold casting and the diameter of the bulk metallic glass was over 20 mm. Some of the Cu-Zr based quaternary alloys with their critical thickness and specific temperatures are shown in the Table 2.4.

Table 2.4 Critical casting diameters and thermal datas of the Cu-Zr based alloys [43]

Alloy Composition (at.%)	$T_g(K)$	$T_x(K)$	$T_l(K)$	$\Delta T_x(K)$	T_g/T_l	ɣ	dc(mm)
$Cu_{45}Zr_{45}Ag_{10}$	683	756	1159	73	0.589	0.410	6
$Cu_{45}Zr_{45}Ag_7Al_3$	688	768	1151	80	0.598	0.418	7
$Cu_{45}Zr_{45}Ag_5Al_5$	697	783	1147	86	0.608	0.425	9
$Cu_{45}Zr_{45}Ag_3Al_7$	708	786	1177	78	0.602	0.417	8
$Cu_{46}Zr_{46}Ag_4Al_4$	686	767	1168	81	0.587	0.414	<7
$Cu_{44}Zr_{44}Ag_6Al_6$	698	790	1144	92	0.610	0.439	10
$Cu_{42}Zr_{42}Ag_8Al_8$	705	780	1213	75	0.581	0.407	12
$Cu_{40}Zr_{40}Ag_{10}Al_{10}$	710	765	1273	55	0.558	0.386	3
$Cu_{40}Zr_{44}Ag_8Al_8$	693	791	1176	98	0.589	0.423	15
$Cu_{36}Zr_{46}Ag_8Al_8$	692	795	1145	103	0.604	0.433	20
$Cu_{36}Zr_{48}Ag_8Al_8$	683	791	1142	108	0.598	0.433	25
$Cu_{34}Zr_{50}Ag_7Al_3$	680	780	1148	100	0.592	0.427	15

2.5 PRODUCTION METHODS OF BULK METALLIC GLASSES

Since the first synthesis, many techniques were sought to produce bulk metallic glasses.

Melt Spinning

In this method, molten metal is driven out an orifice meanwhile the melt is cooled rapidly. Cooling rates are very high, e.g, 10^5-10^6 Ks^{-1} by this way. The dimensions of the products are nearly 2-5 mm in height and 20-50 μm in thickness. [44]
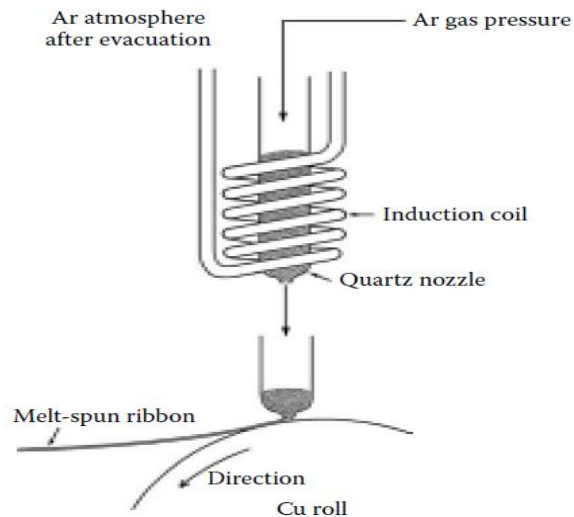
Figure 2.8 Schematic picture of melt spinning method [44]

Flux Melting Technique

In the flux melting technique, the molten oxide flux is used for taking off the impurities which could cause heterogeneous nucleation sites. The melt is both heated and cooled in oxide flux [44]. Kui et.al [45] produced $Pd_{40}Ni_{40}P_{20}$ alloy in glassy state in 10 mm diameter with this method.

Figure 2.9 Schematic representation of Flux melting technique [46]

Water Quenching Method

Water quenching is the simplest process among the other rapid solidification techniques. The alloys are prepared in an induction or arc furnace. Then, they are put into quartz tube where the alloy is completely melted. Finally, the quartz tube is quenched into water. In this method, cooling rates are approximately 10^2 Ks^{-1} [44]. Zhang et.al [47] fabricated $Cu_{36}Zr_{48}Ag_8Al_8$ alloy with 20 mm diameter by water quenching method.

High Presssure Die Casting

High pressure die casting is another method in order to synthesize bulk metallic glasses. The alloy is melted in the sleeve by using induction coil. Following to the melting, the plunger

moves into copper mold and the melt is solidified with flowing cold water [44]. Inoue et.al [12] produced Mg-Cu-Y bulk metallic glass by this method.

Copper Mold Casting

In this popular casting method, the melt is prepared and poured into copper mold where the melt is cooled rapidly. The casting is mainly done in the non-oxidizing atmosphere [44]. Ma et.al [48] produced $Hf_{50}Cu_{30}Ni_{10}Al_{10}$ by using copper mold casting method.

Unidirectional Zone Melting Method

This technique is mainly applied to manufacture of electronic products. The major aim of the unidirectional zone melting is to fabricate pure single crystals. The process involves melting of pure metals along the transverse direction [44].

Suction Casting Method

The other popular method used in bulk metallic glasses forming is the suction casting method. At the beginning step of this process, the alloy is melted into arc melting. Then, the alloy is sucked into copper mold due to the pressure difference between the melting chamber and casting chamber and finally rapid solidified [44]. On the Figure 2.10, the schematic picture of the suction casting is demonstrated. The mold details will be shown in the experimental procedure.
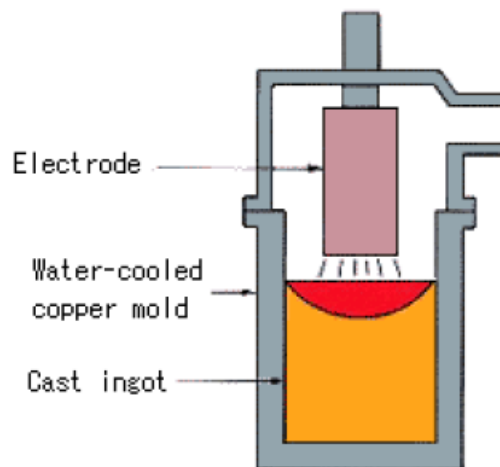
Figure 2.10 The mechanism of suction casting [49]

Arc-Melting Method

By arc-melting technique, material is exposed to an electric arc to melt the alloy on the copper hearth where the melt is solidified with the flowing cold water. This method could be functional for bulk metallic glasses having lower critical cooling rate. One problem of this procedure is obtaining a complete vitreous phase is difficult, since heterogeneous nucleation could be easier between the copper hearth and alloy [44].

2.6 PROPERTIES AND APPLICATIONS OF BULK METALLIC GLASSES

2.6.1 Mechanical Properties

Due to their amorphous structure, bulk metallic glasses are remarked. They do not have slip planes so that they have higher strength than the crystalline alloys [50-52]. A comparison of mechanical features belonging to some materials is indicated on the Figure 2.11.
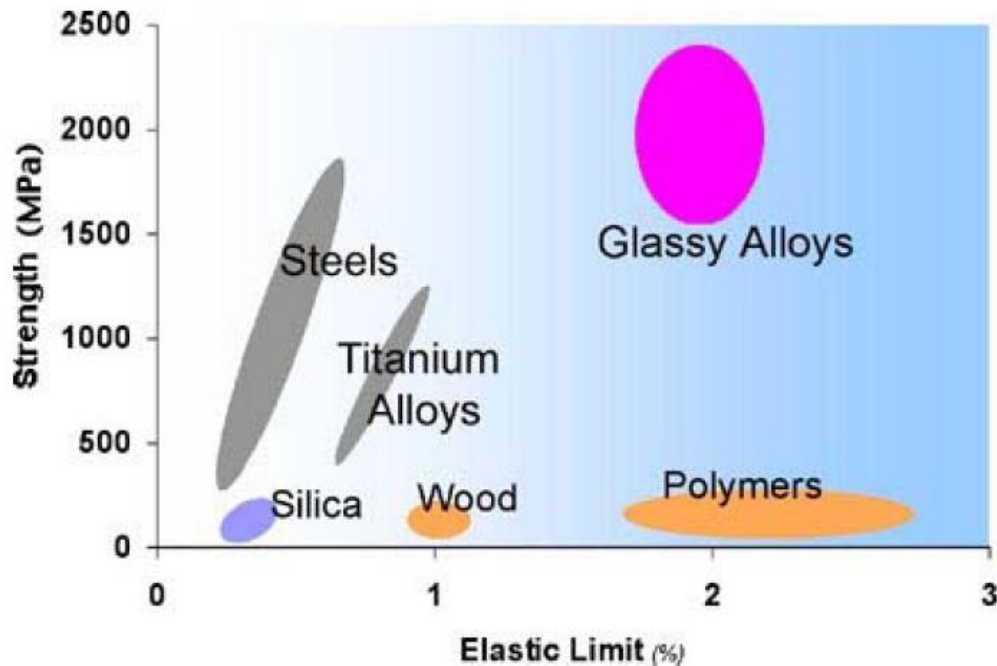
Figure 2.11 Typical strength and elastic limit values for various materials [49]

Bulk metallic glasses have higher strength and more elastic limit values than the other materials. Therefore, this situation makes researchers interest in mechanical properties of the bulk metallic glasses. To get precise information and how amorphous nature affects mechanical properties, the experiments are employed both in as cast state and in annealed state. Stoica et.al [53] explored this situation with the bulk amorphous $Fe_{65.5}Cr_4Mo_4Ga_4P_{12}C_5B_{5.5}$ alloy. The test samples are $2*2$ mm^2 and in 30 mm length. According to their observations, compression strength of the as-cast sample was 2.8 GPA and the strain was 1.9 % with 885 Vickers whereas annealed samples showed 1.6 % strain with 902 Vickers. Jiang et al. [54] studied primary phase effect on bulk amorphous alloys. They examined $Cu_{46}Zr_{47}Al_7$ alloy in monolithic and composite structures. The results indicate that mechanical properties were dependent on the primary phase. The results of their study are given in the Table 2.5.

Table 2.5 The comparison of mechanical properties of monolithic and composite structures of $Cu_{46}Zr_{47}Al_7$ alloy [54]

Sample (mm)	R_c^{Plate} (K/s)	V_{crys} (%)	ε_p (%)	σ_s (Mpa)	$\sigma c,f$ (Mpa)	Structure
1.5	670	0				Glass
2	370	0	6	1894	2250	Glass
2.5	240	4.2	2.97	1890	2056	Glass+CuZr(dendrites)
3	170	8.3	2.11	1817	1933	Glass+CuZr(dendrites)
3.5	120	23.8	0.6	1750	1848	Glass+CuZr(dendrites)
4	90	33.1	3.7	1733	1964	Glass+CuZr(martensite+dendrites)
4.5	70	86.8	2	900	1440	Glass+CuZr+$Cu_{10}Zr_7$
5	60	92.1	2.55	546	1308	Glass+CuZr+$Cu_{10}Zr_7$+Zr_2Cu
6	40	100	3	384	1224	CuZr+$Cu_{10}Zr_7$+Zr_2Cu

2.6.2 Magnetic Properties

Mainly Fe- and Co- based bulk metallic glasses draw attention because of their soft magnetic properties [55]. Due to common industrial applications of Fe-based bulk metallic glasses, the formation and properties of these alloys are researched detailed. Some alloying additions such as Ge,Nb,Si,Co,Cr,Mo have a good effect in stabilizing of the supercooled liquid region of Fe-(Al,Ga)-(P,C,B,Si) bulk metallic glasses and $(Co_{0.705}Fe_{0.045}Si_{0.10} B_{0.15})_{96}Nb_4$ [56]. If Si is added, magnetization properties are enhanced, coercive force is declined and GFA of $Fe_{77}Ga_3P_{12-x}C_4B_4Si_x$ and $Fe_{78}Ga_2P_{12-x}C_4B_4Si_x$ bulk metallic glasses are also enhanced [57].

Recently, Aykol et al. [58] investigated the effect of Cu addition on the magnetic properties of the as-cast and annealed $(Fe_{0.36}Co_{0.36}B_{0.192}Si_{0.48}Nb_{0.04})_{100-x}Cu_x$ alloys. They found that I_s values were decreased with increasing Cu content of bulk metallic glass. They also expressed that annealing developed soft magnetic properties of bulk metallic glass. Figure 2.12 (a) illustrates the I-H loops which indicate that the higher I_s values were obtained by Cu-added annealed BMG. H_c values of the annealed samples were higher than the as-cast state of the samples (Figure 2.12 (b)).
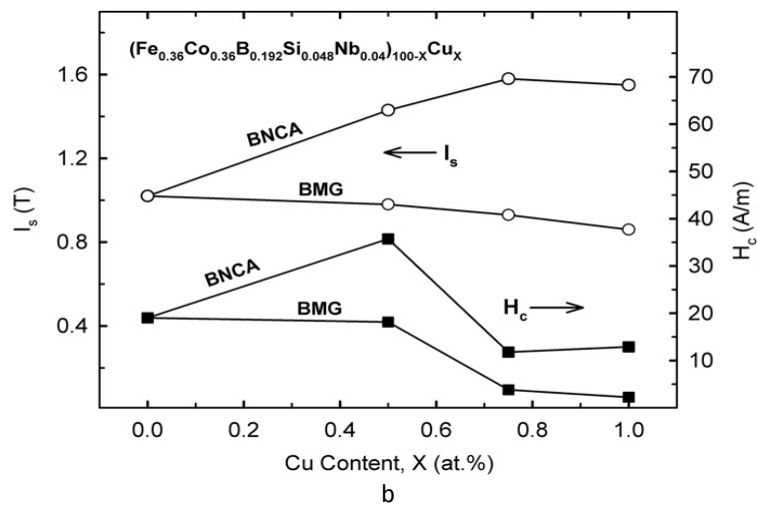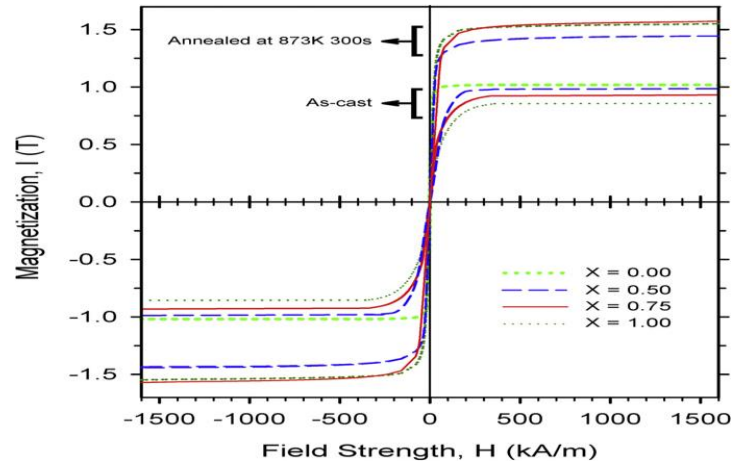
Figure 2.12 a) Hysteresis I-H loops b) Variation of H_s and I_c with Cu content of $(Fe_{0.36}Co_{0.36}B_{0.192}Si_{0.48}Nb_{0.04})_{100-x}Cu_x$ alloys

2.6.3 Chemical Properties

Some elements have been used to enhance the electrochemical and corrosion behaviours of Cu based BMGs. Ta [59, 66], Cr [60, 65] and Mo [59,60,63,66] have some positive impact on electrochemical attitude. Also Nb [59, 61, 62, 64, 66] has positive influence on corrosion behavior. The electrochemical attitude of $Cu_{47}Zr_{11}Ti_{34}Ni_8$ and $(Cu_{47}Zr_{11}Ti_{34}Ni_8)_{99.5}M_{0.5}$ (M=Cr, Mo and W) was studied by Liu et al [60]. They used BMGs with several molar values some specific compound such as H_2SO_4 and NaOH. H_2SO_4 was 0,5 M on the other hand NaOH solutions was 1M. Some elements such as W, Mo and Cr are added to these solutions and good results are obtained. Passive regions are spreaded out, corrosion rates are weakened. Also passive current densities are diminished. Among all solutions, Mo has the best impact on corrosion behavior.

2.6.4 Applications of Bulk Metallic Glasses

Since the first discovery of bulk metallic glasses, many theoretical and experimental investigations were done. In the early works, the dimensions were limited and critical cooling rate was very high. Recently, the formation of centimetersized Zr, Ti, Pd, Pt, Mg, Ln, Fe, Cu and Ni based glassy alloys appeared in some industrial fields. Some appications of bulk metallic glasses are illustrated in Table 2.6 [15].

Table 2.6 Typical Application Fields of Bulk Metallic Glasses [15]

1. Structural
2. Sensor
3. Precision Machinery
4. Optical
5. Ornamental
6. Spring
7. Sporting goods
8. Wear-resistant coating
9. Precision nozzle
10. Corrosion resistant
11. Magnetic
12. Micro-technology
13. Nano-technology
14. Information data storage
15. Biomedical
16. Medical instrument
17. Fuel-cell separator

2.7 CRYSTALLIZATION KINETICS

2.7.1 Isochronal Crystallization Kinetics

The basic rule of the isochronal crystallization kinetics is the shift of crystallization and glass transition peaks as the heating rate increases. The well-known equations are Kissinger and Ozawa methods. Nevertheless, there are some studies related to isochronal crystallization kinetics. Kissinger approach [67] was shown below:

$$ln\left(\frac{\beta}{T_{p}^{2}}\right) = \frac{-E}{RT_p} + A \tag{2.8}$$

where β is the scanning rate in (K/s), R is the universal gas constant, T_p is the peak temperature of crystallization in (K/s) and A is constant. By using equation (2.8), ln (β/T_p^2) versus $1000/T_p$ graph is drawn in order to find the activation energies of glass transition and crystallization from the slope. An example of Kissinger plot is shown in the Figure 2.13.
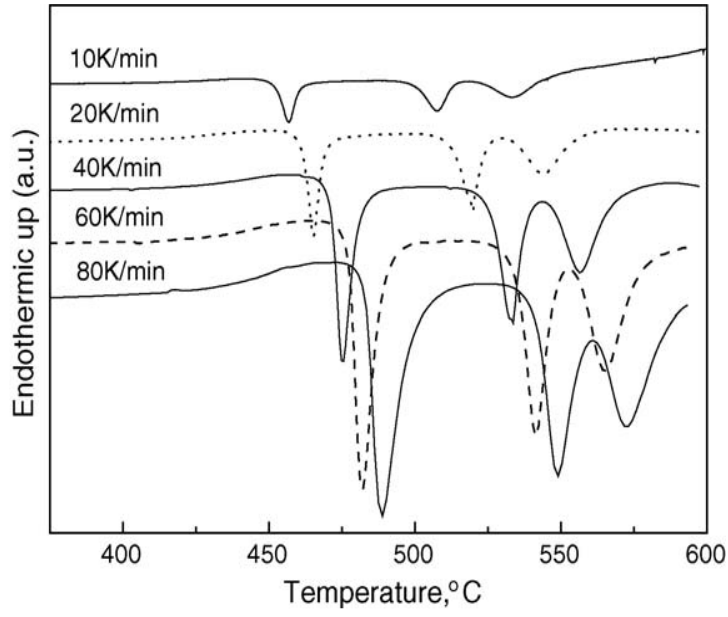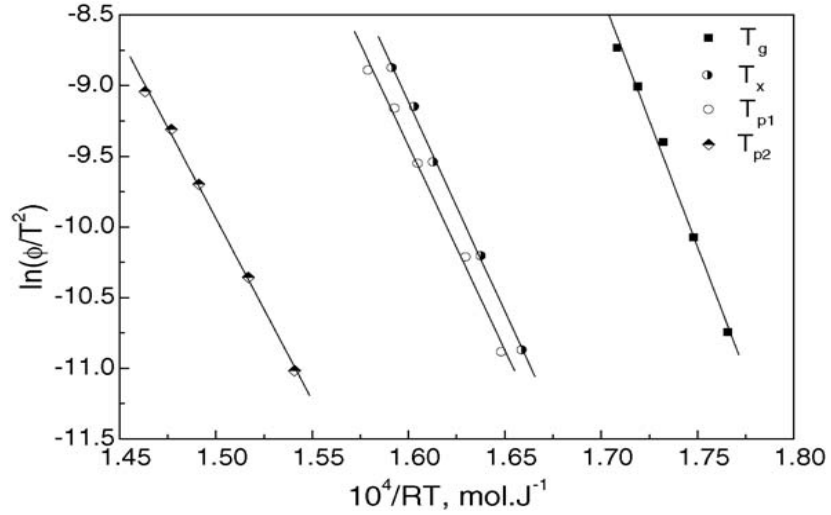
Figure 2.13 a) DSC curves of the bulk amorphous $Cu_{52.5}Ti_{30}Zr_{11.5}Ni_6$ alloy at different heating rates b) Kissinger plots of the bulk amorphous this alloy [68]

Another popular method is Ozawa Method [69]. By this method $\ln\beta$ versus $1000/T_p$ curve is obtained. The slope gives the activation energy.

$$ln\,\beta = \frac{-1.0516E}{RT_p} + A \tag{2.9}$$

The other way to determine the activation energies was developed by Boswell [70] which is exhibited as:

$$ln\left(\frac{\beta}{T_p}\right) = \frac{-E}{RT_P} + const. \tag{2.10}$$

Barandiaran and Colmenero [71] developed a method in order to estimate the critical cooling rate based on isochronal crystallization kinetics.

$$ln\ R = ln\ R_c - \frac{B}{(T_l - T_{xc})^2} \tag{2.11}$$

where R is cooling rate, T_l is the offset temperature of fusion and T_{xc} is the onset temperature of solidification.

2.7.2 Isothermal Crystallization Kinetics

DSC or DTA measurements play an important role for crystallization kinetics. Johnson-Mehl-Avrami equation [72-74] is applied to isothermal crystallization kinetics. The equation is:

$$X = 1 - exp[-k(t - \tau)^n] \tag{2.12}$$

where x is crystallized volume fraction, τ is incubation time, t is annealing time, n is Avrami exponent and k is reaction constant.

The values of k and n could be calculated by using below equation [75]

$$ln\left[ln\left(\frac{1}{(1-x)}\right)\right] = n\ lnk + n\ ln(t - \tau) \tag{2.13}$$

The details of the crystallization kinetics can be understood by computing local Avrami exponent [76]:

$$n(x) = \frac{\partial\ ln\left\{ln\left[\frac{1}{(1-x)}\right]\right\}}{\partial\ ln\ (t - \tau)} \tag{2.14}$$

Liu et al. [77] studied the isothermal crystallization kinetics of $Zr_{55}Cu_{30}Al_{10}Ni_5$ bulk amorphous alloy. They found both activation energy and kinetic parameters with plotting $ln[ln(1/(1-x))]$ versus $ln(t-\tau)$ and lnk versus $1000/T(K^{-1})$ graphs, Figure 2.14.
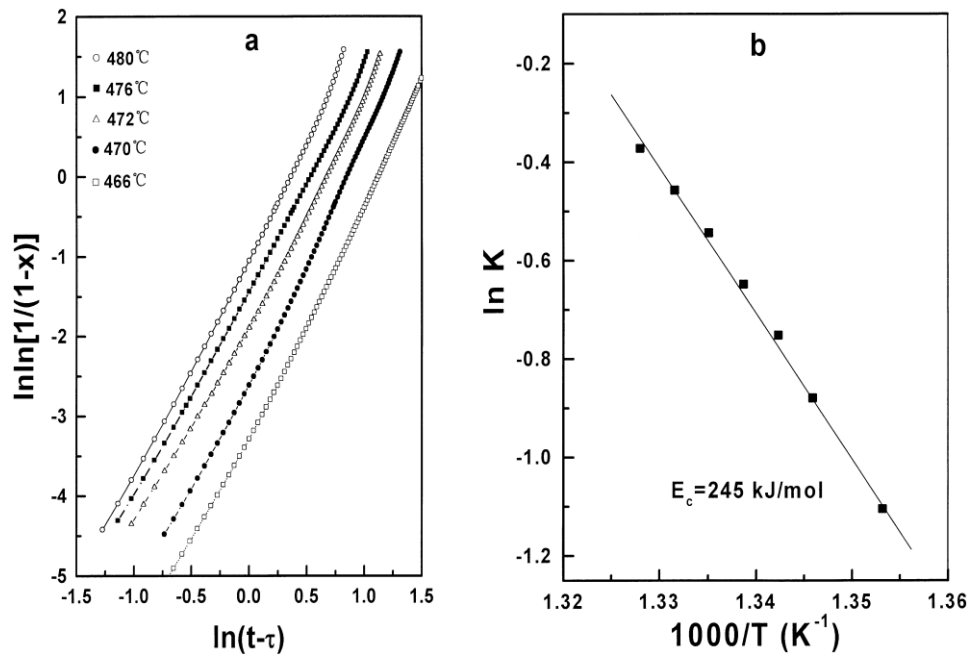
Figure 2.14 a) JMA plots for the crystallization at different temperatures, (b) ln k vs. $1/T$ plot of the $Zr_{55}Cu_{30}Al_{10}Ni_5$ bulk amorphous alloy [77]

2.7.3 Nanocrystallization

Nanocrystalline structures are one of the most attractive products of bulk glass forming alloys. Recently, nanocrystalline materials began to take place much in scientific studies. Some works proved that nanocrystalline materials have better mechanical properties than the amorphous metallic alloys [78]. There are different methods to acquire nanocrystals. One is known as conventional nanocrystallization. In this method, metallic glass is exposed to isothermal annealing close to peak temperature of crystallization. The other ways are high temperature annealing also named as flash annealing [79, 80] and low temperature annealing [81]. Koster et al [82] produced nanocrystals in $Zr_{50}Co_{50}$ alloy through high temperature annealing technique. Gao et al. [83] synthesized nanocrystals in amorphous matrix of $Zr_{41.2}Ti_{13.8}Cu_{12.5}Ni_{10}Be_{22.5}$. Figure 2.15 shows the TEM images of their work.

Figure 2.16 is related to the temperature dependence of nucleation and growth rate. There could be an increment of nucleation rate instead the growth rate if the annealing temperature is increased. This difference induces finer structure at high temperature crystallization. In addition, the compositions of nanocrystallization products are affected by the annealing temperature and annealing time. Composition of crystals deviates from the original composition of the alloy due to lower annealing temperature and less time [84].

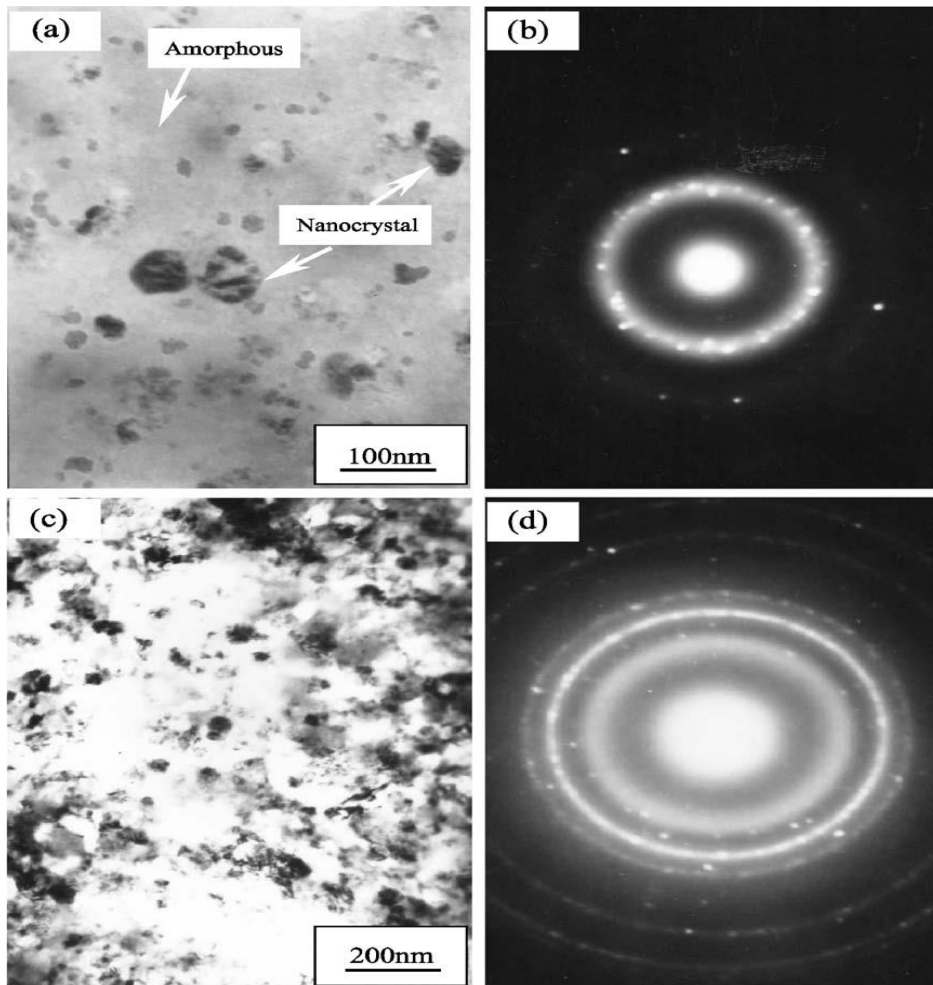Figure 2.15 The TEM images and corresponding selected area diffraction patterns corresponding to the first (a, b) and second crystallization reaction (c, d) of $Zr_{41.2}Ti_{13.8}$ $Cu_{12.5}Ni_{10}Be_{22.5}$ bulk metallic glass at 430 °C [83].
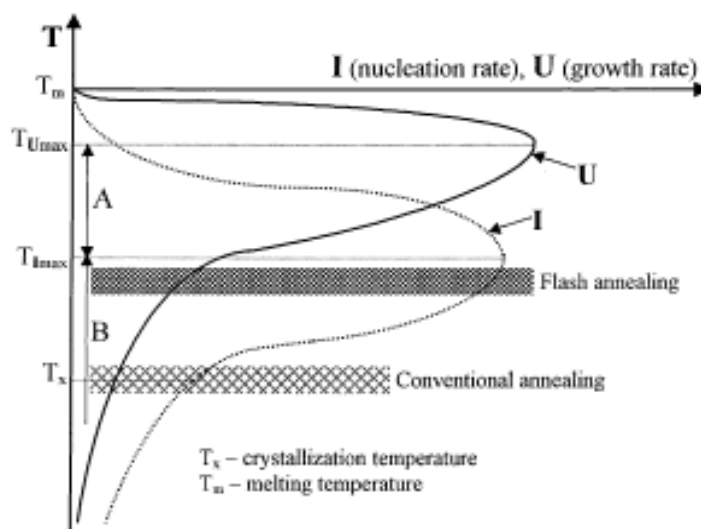
Figure 2.16 Schematic view of the the relationship between temperature and growth rate U and nucleation rate I [84]

CHAPTER 3

EXPERIMENTAL PROCEDURE

3.1 ALLOY PREPARATION

3.1.1 Raw Materials

Cu, Hf, Al, Zr and B are used as the starting materials to prepare the alloys. Their purities are given in the Table 3.1.

Table 3.1 Purities of elements used for alloy preparation

Element	Purity
Cu	99.99 %
Hf	99.97 %
Al	99.99 %
Zr	99.98 %
B	99.95 %

All the elements were cut into small pieces for convenience alloy preparation.

3.1.2 Alloy Preparation

Samples were prepared by arc melting technique using a water- cooled copper hearth and non-consumable tungsten electrode in Zr-gettered argon atmosphere. In order to achieve chemical homogeneity, alloys were remelted three times. The weight loss during arc melting process was smaller than 0,5 wt%. Finally, a rod like shaped master alloy ingot was obtained. The photos of final products are given on the Figure 3.1.

For the characterization, the master alloy was cut into 1.5 mm slices by wire-erosion machine. Suction casting method was used for rapid solidification. In this method while ingot is melted, the valve is opened; generating a vacuum in the chamber and finally the molten metal is sucked into a cylindrical copper mold. The technical drawing of copper mold is given on the Figure 3.2.

a   b

Figure 3.1 a) The product prepared by arc melting b) The product prepared by suction casting.

Figure 3.2 Technical drawings of copper mold

3.2 CHARACTERIZAION TECHNIQUES

Metallographic Examination

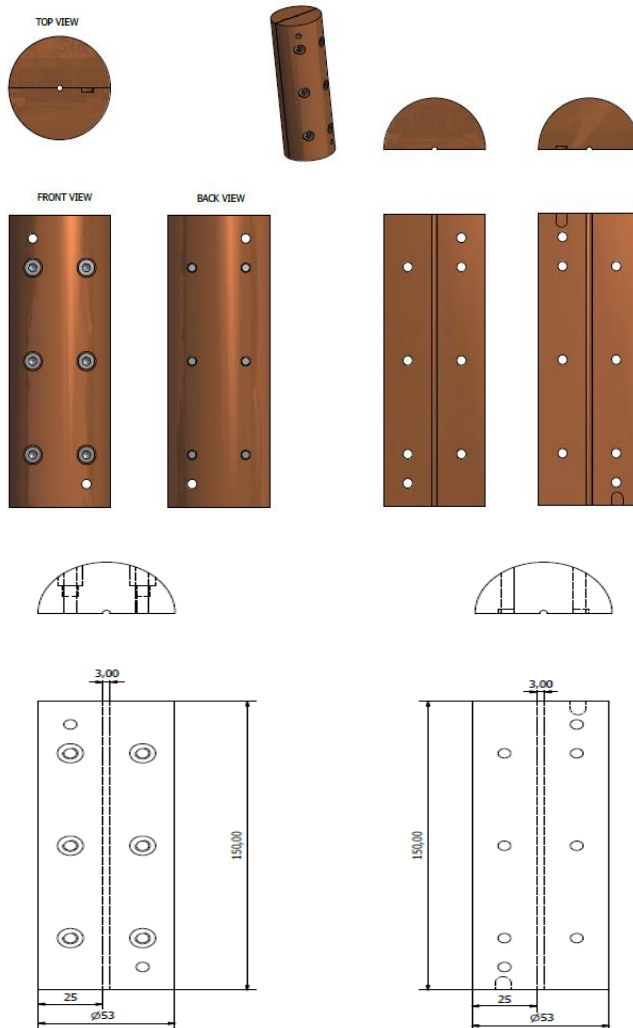The microstructural examination was performed using Nikon Optihot Light microscope, JEOL JSM-6400 Scanning Electron microscope (SEM) and FEI NOVA NANOSEM. The samples were mounted into bakalite, ground with SİC emery papers up to 1200 grit and polished. % 0.5 HF was used as etchant.

Thermal Analysis

Setaram SETSYS 16/18 differential scanning calorimeter (DSC) thermal analyzer was used for thermal analysis. Each sample was cut into a small piece weightiness between 20-30 mg and put into alumina crucible. In order to avoid sticking the sample into the crucible, alumina powders were placed also into crucible. Temperature calibration was done using reference materials of Zn, Ag, Al and Ni. For the specimens, scanning rate between 5-99 °C/min was used. The slow scannig rate is advantegous since rapid scannig rates can obscure thermal events. The data about the heat flow and temperature were acquired from the DSC system. The thermal behaviour of alloys is understood from the DSC analysis. If heat absorbed events occur such as solid solid transitions and melting, they are observed as endothermic on the DSC curve. However, if heat released cases happen such as crystallization and decomposition, they are observed as exothermic on the DSC curve. Both of the invariant temperatures and enthalpies are also acquired from the DSC curve.

X-Ray Diffraction

X-ray diffraction (XRD) analysis was done using a Rigaku D/max-22000C diffractometer with CuK_{α} radiation with a wavelength of 1,54 Å. The experimental parameters were 40 kV voltages and 30 mA current. The x-ray datas were obtained as 2Ɵ between 20° and 100°.

Hardness Measurements

Vickers Hardness measurement method was employed in order to investigate hardness of alloys. For the Vickers test, square-based diamond pyramidal indenter was used. The test load applied to specimens was 1 kgf. The test instrument is EMCO Universal Hardness Testing Machine.

CHAPTER 4

RESULTS AND DISCUSSIONS

The aim of the study is to synthesize and characterize copper based bulk metallic glasses. First, the solidification behaviors of binary Cu-Hf based binary alloys are presented in Section 4.1. The formation of $Cu_{49}Hf_{42}Al_9$ amorphous alloy is presented in Section 4.2. The results of crystallization kinetics are shown in Section 4.3. The samples were characterized using the techniques, described in Section 3.

4.1 The Solidification Behaviour Cu-Hf binary alloys

4.1.1 The Solidification Behaviour of $Cu_{70}Hf_{30}$ alloy

70 at% Cu – 30 at%Hf binary alloy was chosen as starting alloy of the experimental studies since the alloy at this composition goes a sequence of peritectic and eutectic reactions which was found to be important parameter for high bulk glass forming ability [32]. The phase diagram of Cu-Hf is given on the Figure 4.1.
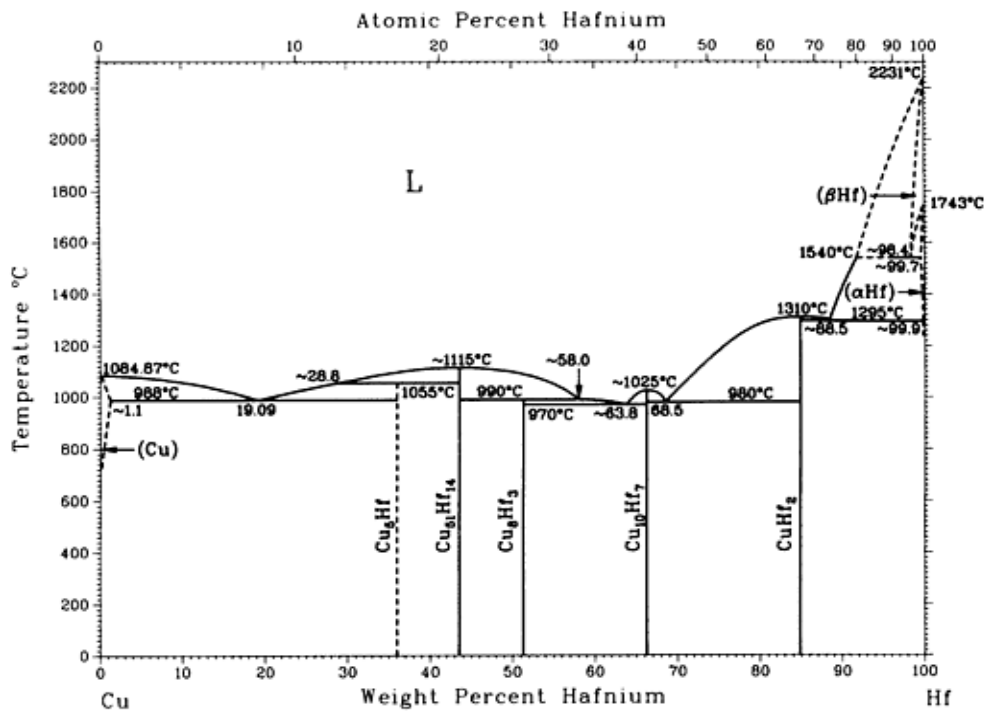

Figure 4.1 The Cu-Hf phase diagram

$Cu_{70}Hf_{30}$ alloy was synthesized by arc melting. Usage of arc melting method caused non-equilibrium solidification circumstances. As-cast samples were cut by a wire-erosion machine. The schematic drawing of the sample is given on the Figure 4.2.
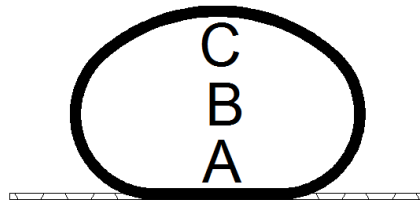

Figure 4.2 The schematic drawing of as-cast slice. The letters indicate examined regions and the dashed lines show the contact surface between the sample and arc melting unit

The ingot slice was in contact with the copper hearth of arc melting device. The contact area is the most fastly cooled part of the sample. For this reason, distinct microstructural aspects are anticipited.

The microstructure of the alloy was studied along the sample in order to analyze the changes due to variable cooling rates. The SEM photos and EDS analysis are given in the Figure 4.3 and Table 4.1. The phases were identified according to XRD pattern, phase diagram and EDS analysis. The lightest contrasted phase is $Cu_{51}Hf_{14}$. On the other hand, the darkest contrasted phase surrounding this phase is Cu_8Hf_3. The medium contrasted phase is Cu_5Hf. If the results were correlated with Cu-Hf phase diagram, the solidification process could be comprehended. $Cu_{51}Hf_{14}$ phase appeared as primary phase in the first stage of solidification. Then, Cu_8Hf_3 phase formed due to peritectic reaction and the remainig liquid transformed into Cu_8Hf_3 and $Cu_{10}Hf_7$ at the eutectic point.

When comparing the SEM photos, effects of cooling rate on microstructures can be seen obviously. Cu_5Hf phase was appeared only in the contact area. Although this phase was not expected from the phase diagram at this composition, such a compositional shift is comprehensible in the non-equilibrium conditions. Also, the morphologies of eutectic structure and primary phase became more irregular in the fastly cooled regions. It is generally known that higher cooling rate results in fine microstructures, but the situation is different here. The structure of $Cu_{51}Hf_{14}$ became coarser in the high undercooled region. Yang et al. [85] explained this case with classical nucleation theory. According to this theory, two exponential terms, which are the activation energy for the formation of critical nuclei and driving force for the atomic diffusion process, control the nucleation rate. At small undercoolings, activation energy for the formation of critical nuclei dominates, which result in the increase of nucleation rate. At high undercoolings, the driving force for atomic diffusion process dominates, which result in the decrease of nucleation rates [86]. Thus, high undercooling causes high growth velocity so grains become coarser [85].

28

a

b

c
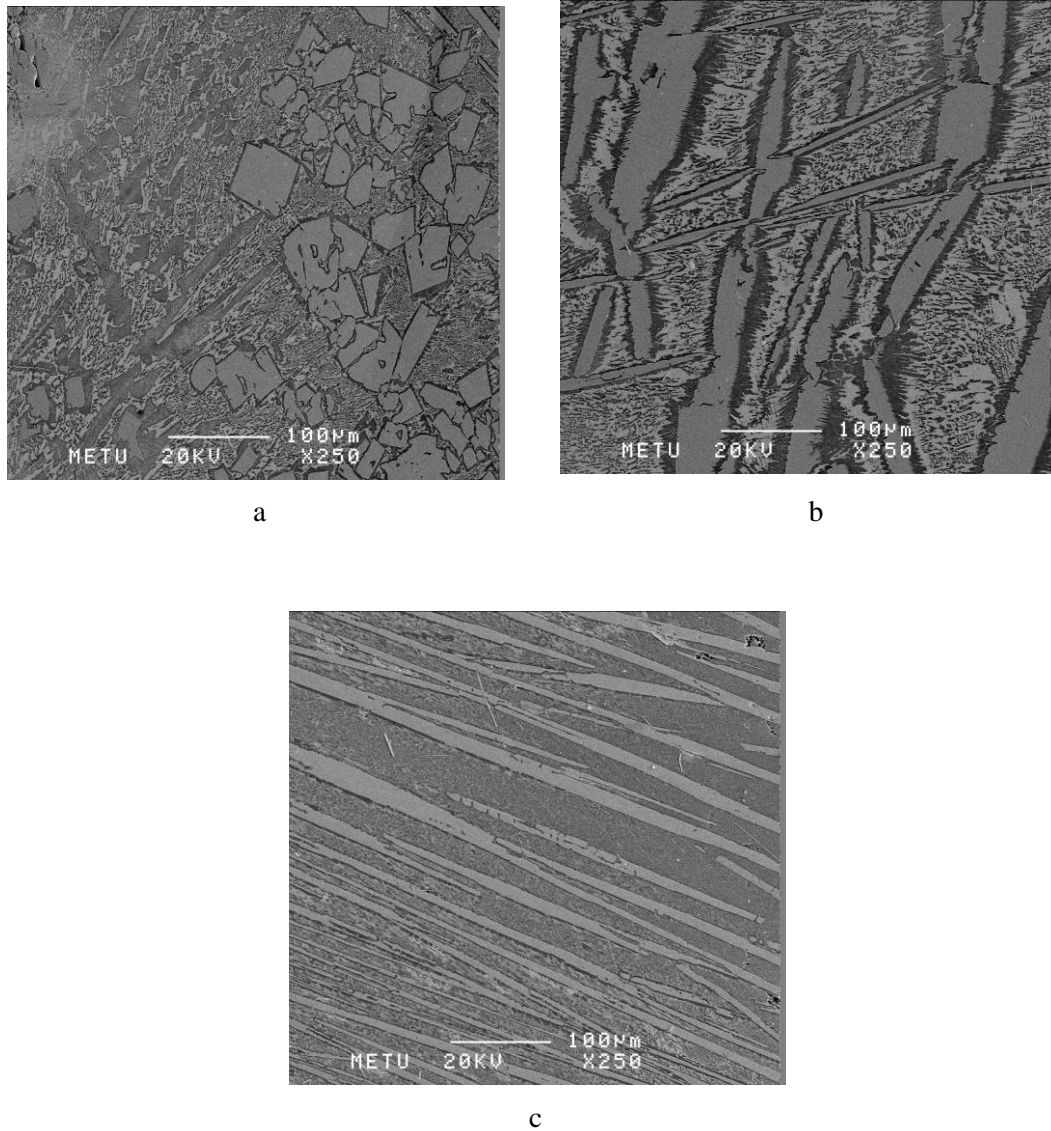
Figure 4.3 Secondary electron images of $Cu_{70}Hf_{30}$ alloy a) region A, b) region B, c) region C

Table 4.1 EDS analyses of $Cu_{70}Hf_{30}$ alloy

Phase	Element	Atom (%)
Ligthest contrasted phase	Cu	79.90
	Hf	20.10
Medium contrasted phase	Cu	86.07
	Hf	13.93
Darkest contrasted phase	Cu	71.43
	Hf	28.57

Figure 4.4 X-ray diffraction pattern for $Cu_{70}Hf_{30}$ alloy

Isochronal DSC thermogram is given in Figure 4.5. This curve shows eutectic, peritectic and melting sequences.
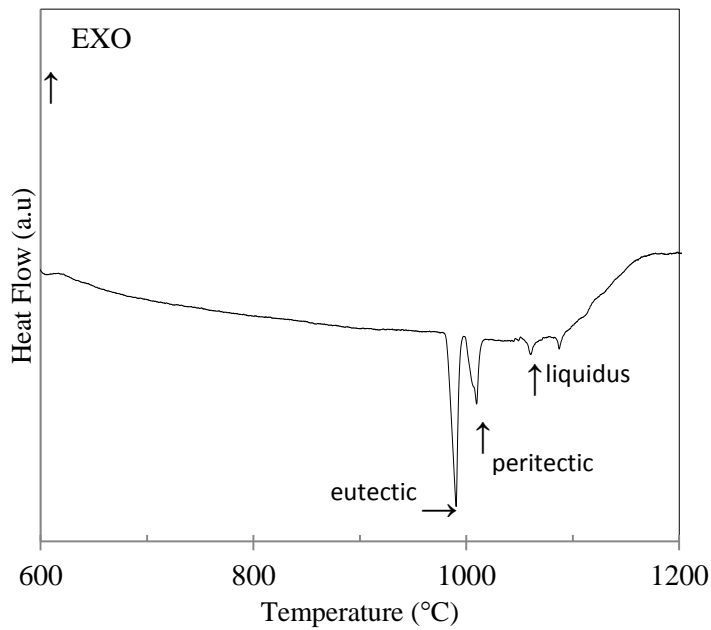
Figure 4.5 DSC Heating curve for $Cu_{70}Hf_{30}$ alloy at a rate of 10°C/min

Table 4.2 DSC datas of the $Cu_{70}Hf_{30}$ alloy

Alloy	T_e (°C)	T_p (°C)	T_l (°C)	ΔH_e (j/g)	ΔH_p (j/g)	ΔH_l (j/g)	$\Delta H_p / \Delta H_e$
$Cu_{70}Hf_{30}$	990	1010	1060	26.2	11,8	3,9	0.45

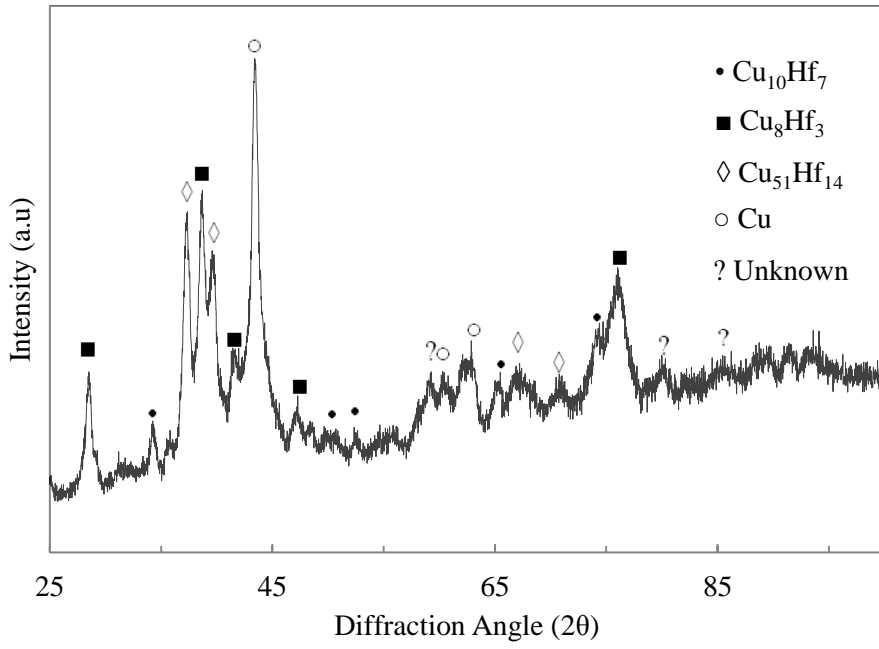The temperatures of invariant reactions of as-cast sample are nearly 20°C higher when compared with the equilibrium phase diagram of Cu-Hf. This case is related to non-equilibrium solidification since arc melting provides higher undercooling than solidifying the alloy into stable phases.

The effect of cooling rate on the properties of the $Cu_{70}Hf_{30}$ alloy can also be seen from the hardness curve given in the Figure 4.6. If cooling rate increases from the region C to region A, the strength increases too.

Figure 4.6 The hardness values along the as cast sample

Schematic view of the sample

4.1.2 The Solidification Behaviour of Cu$_{50}$Hf$_{50}$ alloy

In order to understand glass forming ability of binary alloys, 50 at% Cu-50 at% Hf alloy was prepared. This composition was chosen 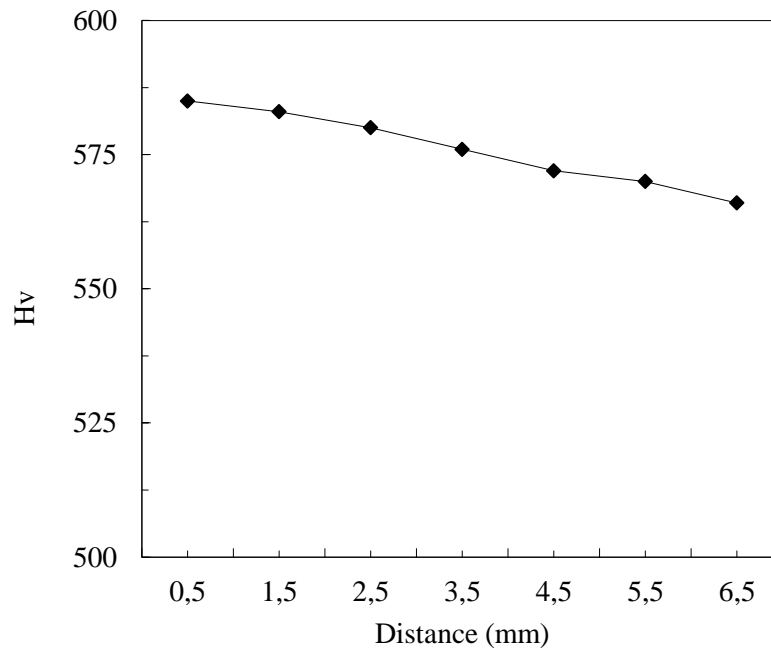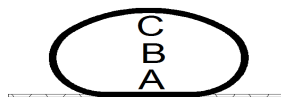on right-hand-side of the congruent point since the alloy goes eutectic reaction which is favorable for high glass forming ability. Cu$_{50}$Hf$_{50}$ alloy was also synthesized by arc melting. Secondary electron images are shown on the Figure 4.7

a   b
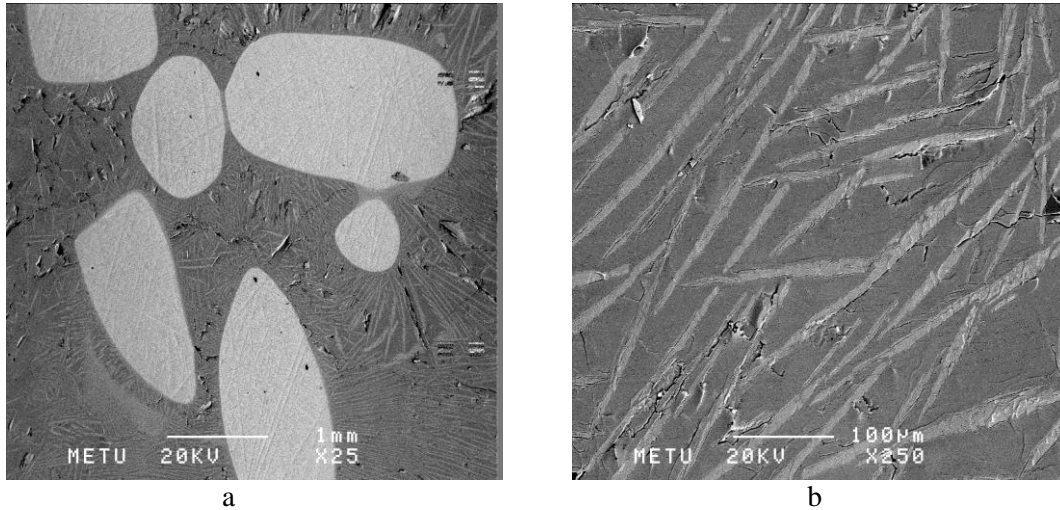
Figure 4.7 Secondary electron images of Cu$_{50}$Hf$_{50}$ alloy a) general view
b) detailed view

Considering the binary Cu-Hf phase diagram, a primary phase and eutectic mixture of Cu$_{10}$Hf$_7$+ CuHf$_2$ would be expected. When microstructure of the alloy was examined, neither all phases nor eutectic structure were existed. Lightest contrated phase was thought to be an unmelted phase. Medium contrasted phase is one of the anticipitated phases. According to EDS analysis and XRD results the phases were identified as Hf and Cu$_{10}$Hf$_7$. XRD pattern is demonstrated on the Figure 4.8.

All these results implied that alloy preperation was very difficult due to more hafnium addition. Furthermore, the alloy was oxidized due to applied more arc.
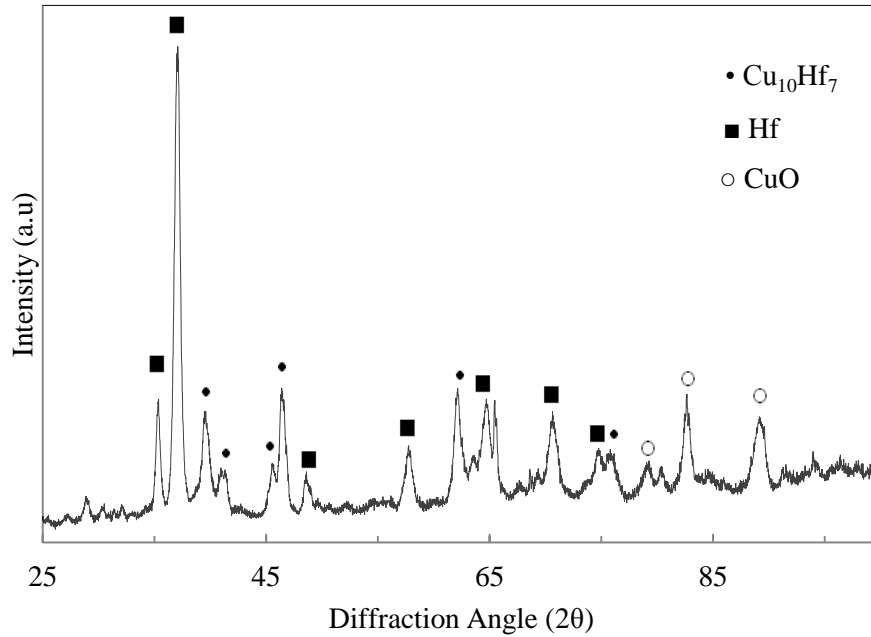
Figure 4.8 XRD pattern of $Cu_{50}Hf_{50}$ alloy

4.2 Bulk Metallic Glass Formation

4.2.1 Rapid Solidification Behavior of the $Cu_{49}Hf_{42}Al_9$ alloy

It is generally known that it is easier to synthesize glassy phases in higher-order alloy systems than in binary and ternary alloy systems. The results of Section 4.1 also confirmed this idea since amorphous structure was not obtained by using binary compositions although they were prepared by arc melting. Therefore, an attempt was made by adding aluminum to Cu-Hf binary system. $Cu_{49}Hf_{42}Al_9$ alloy was synthesized by suction casting in order to obtain amorphous structure. Secondary electron images of this alloy are given in the Figure 4.9. The photos were taken from the center and near the mold region of the sample. Homogeneous contrast could be seen from the SEM images. Also, there is no visible crystal which is indicator of achieving amorphous structure.
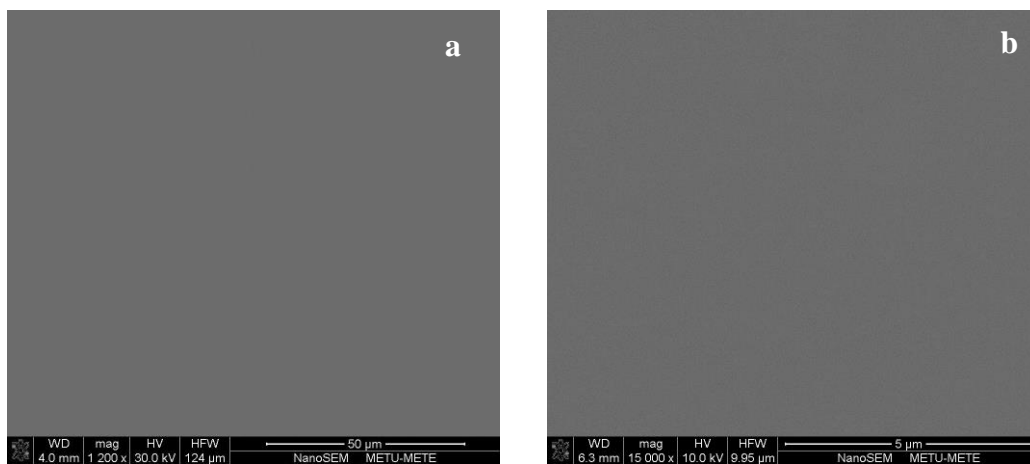
Figure 4.9 Secondary electron images of the $Cu_{49}Hf_{42}Al_9$ amorphousalloy a) near mold region b) center region

33

Further examinations on the $Cu_{49}Hf_{42}Al_9$ alloy were conducted by XRD and thermal analysis. The XRD results are shown on the Figure 4.10.
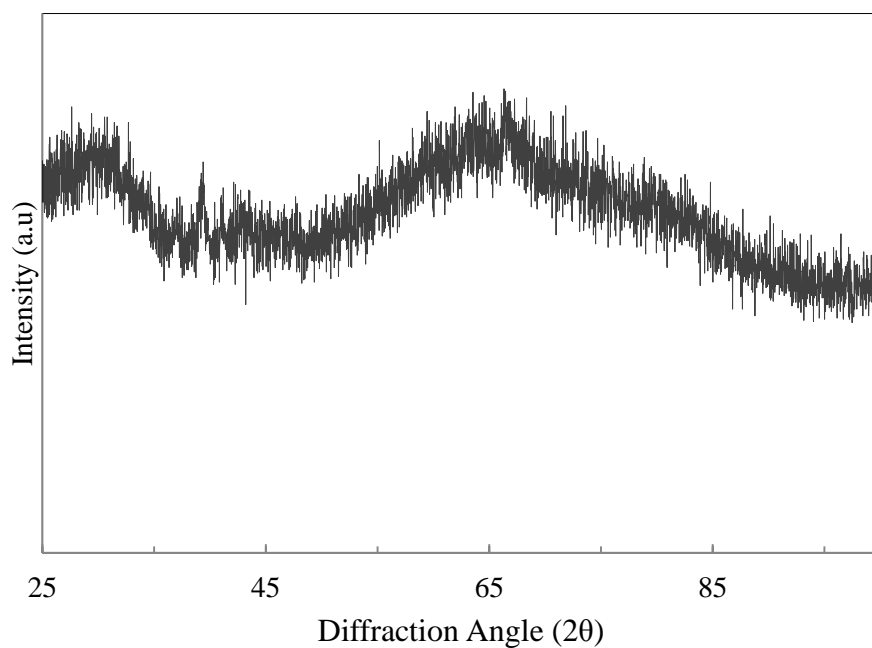
Figure 4.10 XRD pattern of the amorphous $Cu_{49}Hf_{42}Al_9$ alloy

The XRD pattern of this alloy is a characteristic sign of the amorphous nature with broad diffraction maxima. The amorphous nature of the $Cu_{49}Hf_{42}Al_9$ alloy was also confirmed by thermal analysis. The DSC curve is demonstrated on the Figure 4.11.
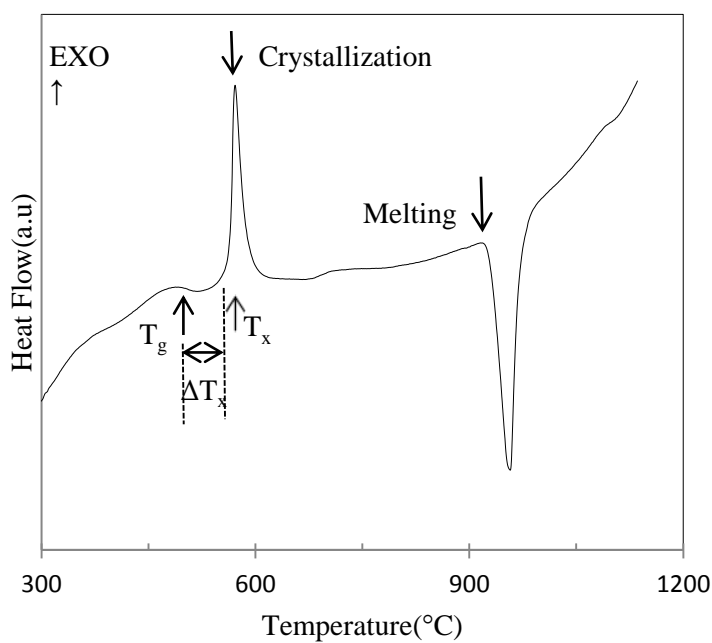
Figure 4.11 DSC thermogram of the $Cu_{49}Hf_{42}Al_9$ alloy scanned at a rate of 40 °C/min

Table 4.3 Thermal datas of the $Cu_{49}Hf_{42}Al_9$ alloy

Alloy	T_g (°C)	T_x (°C)	T_m (°C)	ΔT_x(°C)	ΔH_x(kj/mol)	ΔH_l (j/g)
$Cu_{49}Hf_{42}Al_9$	507	571.36	929.25	64	-25,79	46,71

Figure 4.11 shows a sharp crystallization peak and a clear glass transition. The alloy was successfully crystallized in one stage. The T_g, T_x, ΔH_x and ΔT_x values are indicated in table 4.5. The extention of the supercooled region is 64 °C while T_{rg} is 0.59. These values are in good agreement with the results reported in the literature [41].

Compression test and hardness measurements were conducted in order to investigate the mechanical properties of the $Cu_{49}Hf_{42}Al_9$ alloy. The hardness profile was given in the Figure 4.12 and pre-experimental results of the compression test are illustrated on the Figure 4.13. The values represent that the alloy has strength over 600 Hv, 1600 MPa compressive stress and 4 % compressive strain.
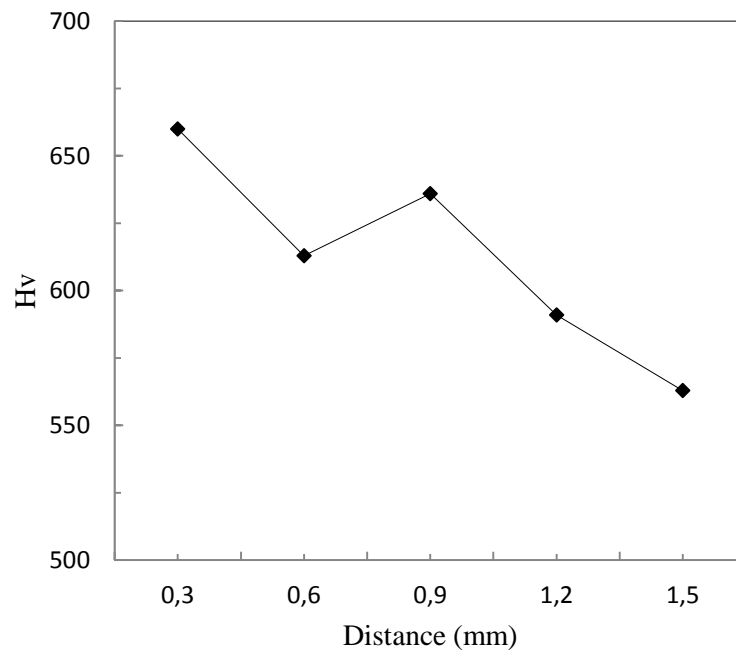
Figure 4.12 The Hardness profile of the amorphous $Cu_{49}Hf_{42}Al_9$ alloy

Schematic view of the sample
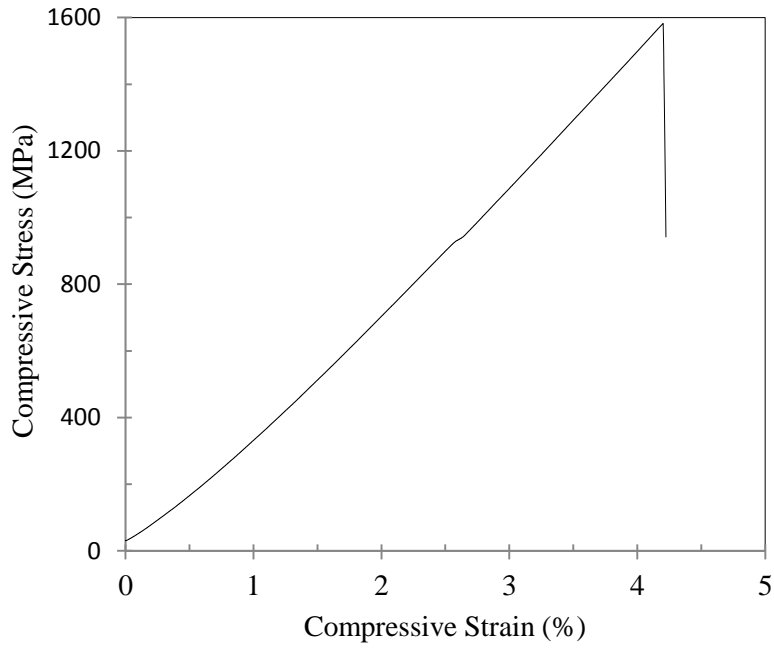
Figure 4.13 Compressive Stress-Compressive strain diagram of amorphous $Cu_{49}Hf_{42}Al_9$ alloy

4.2.2 Near Equilibrium Solidification Behaviour of $Cu_{49}Hf_{42}Al_9$ Alloy

A near equilibrium sample was synthesized in order to get information about the solidification behavior of $Cu_{49}Hf_{42}Al_9$ alloy. The sample was first slowly heated to above melting point and then kept at that temperature nearly half an hour. Finally, the alloy was slowly cooled to room temperature in the DSC furnace. The resultant microstructures are indicated on the Figure 4.14.

a

b
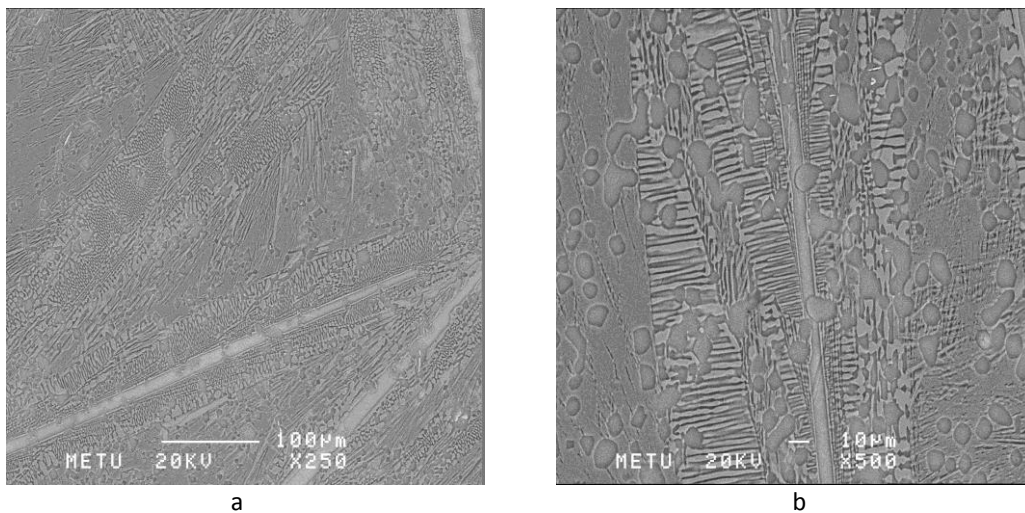
Figure 4.14 Secondary electron images of the near-equilibrium sample of
$Cu_{49}Hf_{42}Al_9$ alloy a) general view b) detailed view

The phases were determined according to phase diagram, EDS analysis and X-ray diffraction pattern. White contrasted phase was developed as primary phase. This phase is Cu_8Hf_3. However, this phase would not be expected at that composition of the Cu-Hf phase diagram. According to Subramanian et al [87], formation of Cu_8Hf_3 is more thermodynamically favorable than the other phases. For this reason, Cu_8Hf_3 might be devoloped as primary phase. Spherical shape phase was predicted to be $Cu_{51}Hf_{14}$ and lamellar eutectic structure was formed by coprecipitation of Cu_5Hf and Cu_2AlHf. This immediately implied that the suppression of eutectic reaction during solidification resulted in formation of an amorphous structure. Neverthless, Jia et al studied the solidification microstructures at a cooling rate just below the critical rate for glass formation [42]. They found that the $Cu_{49}Hf_{42}Al_9$ alloy had ternary eutectic structure which is composed of $Cu_{10}Hf_7$, $CuHf_2$ and $CuHfAl$ and had a $CuHf_2$ as primary phase. All the results implied that mainly Cu rich phases of Cu-Hf system were formed in the near equilibrium sample. The mechanism beyond these phases was not comprehended clearly.This might be arisen from the alteration of kinetic pathways during relaxation towards equilibrium. Alternatively, liquid–solid interfacial energy of Cu-rich intermetallics could be less which might favor formation of Cu-rich phases. DSC analysis is given on the Figure 4.15.
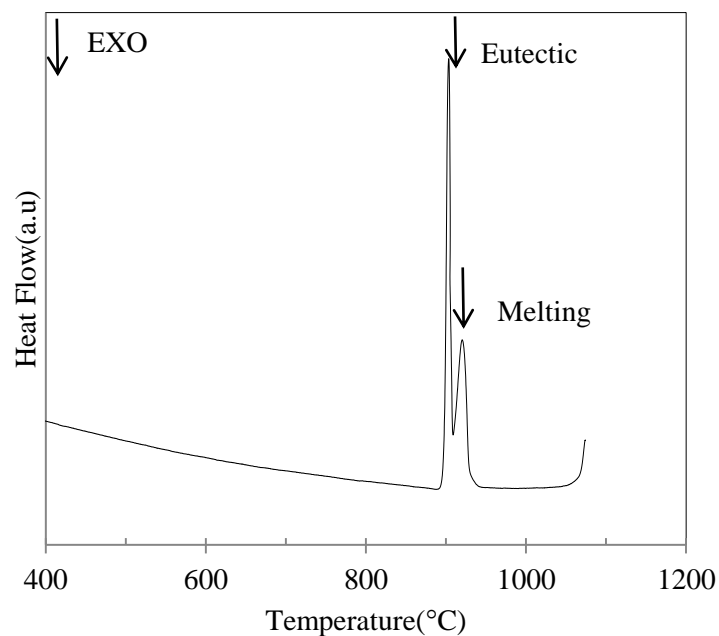
Figure 4.15 The DSC patterns of near-equilibrium sample of the $Cu_{49}Hf_{42}Al_9$ alloy scanned at a rate of 10˚C/min (Cooling Curve)

The eutectic temperature of near equilibrium $Cu_{49}Hf_{42}Al_9$ alloy was estimated to be 910°C from DSC curve. This value was compared with hypereutectic region of the Cu-Hf phase diagram. It was noticed that the eutectic temperature was dropped nearly 70°C. As a result, Aluminum addition stabilized the melt and caused deep eutectic. Hence, glass forming ability was favored.

XRD results are shown on the Figure 4.16.
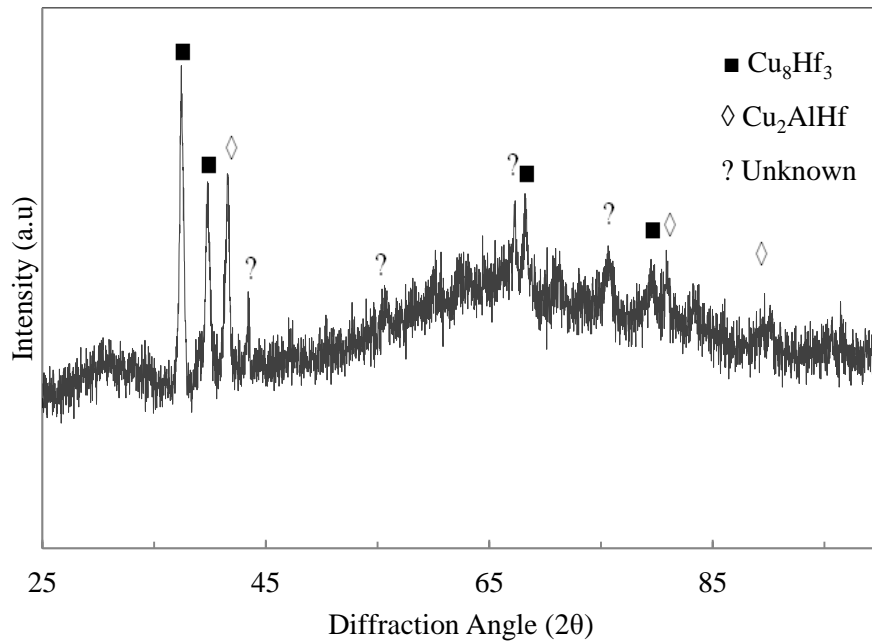
Figure 4.16 XRD pattern of near-equilibrium sample of the $Cu_{49}Hf_{42}Al_9$ alloy

4.3 Crystallization Kinetics of the $Cu_{49}Hf_{42}Al_9$ Alloy

Crystallization kinetics study is an important study to get information about GFA and the mechanism of phase transformation. Nanocrystallization studies are important for bulk metallic glasses to acquire better properties such as mechanical. This purpose makes the researches comprehend the thermal stability and microstructural features of crystallization of amorphous alloys. However, there are a few studies on the crystallization kinetics of Cu based bulk metallic glasses. For this reason, the crystallization kinetics of the $Cu_{49}Hf_{42}Al_9$ amorphous alloy will be examined in isochronal and isothermal conditions.

4.3.1 Isochronal Crystallization Kinetics of the $Cu_{49}Hf_{42}Al_9$ Alloy

The isochronal crystallization kinetics of $Cu_{49}Hf_{42}Al_9$ alloy was studied by differential scanning calorimetry. This part consists of both critical cooling rate and activation energy surveys. The activation energies of glass transition and crystallization were estimated by Kissinger approach which is based on peak shifts of thermodynamic temperatures obtained from DSC thermograms [67]. Therefore, the DSC experiments were done at different heating rates starting from 5°C and ending up with 99°C. The DSC thermograms are shown on the Figure 4.17.
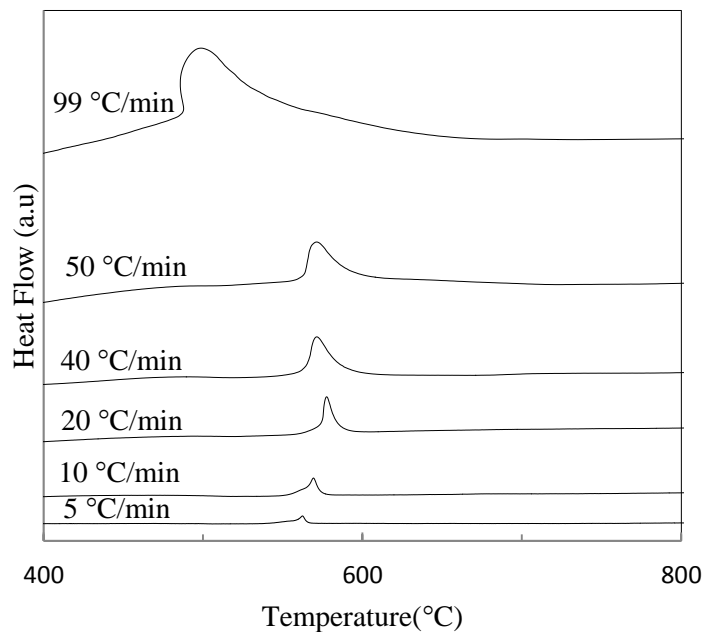
Figure 4.17 DSC Thermogram of heating rates of 5°C/min up to 99°C/min

DSC thermogram results imply show that as the heating rate was increased; the height of peak, i.e intensity was increased due to high sensitivity at high scanning rates. In order to apply Kissinger approach, peak shifts are taken into consideration. However, the curves at 40°C, 50°C and 99°C do not follow Kissinger approach. Therefore, the curves were ommitted while calculating the activation energies. Therefore, DSC heating curves at 5°C, 10°C and 20°C were evaluated. The labeled DSC curves are shown on the Figure 4.18 and thermal data are given in the Table 4.4.

Figure 4.18 DSC thermograms of the scanning rates of 5°C/min, 10 °C/min and 20°C/min
(Heating Curves)

Table 4.4 Thermodynamic Temperatures at the heating rates of
5°C/min, 10 °C/min and 20°C/min

Scanning Rate (°C/min)	T_g(°C)	T_x(°C)	T_p(°C)
5	506.51	557.61	562.29
10	515.75	561.96	571.67
20	519.46	573.84	577.60

The Kissinger plot was drawn and activation energies were calculated taking these values into consideration.
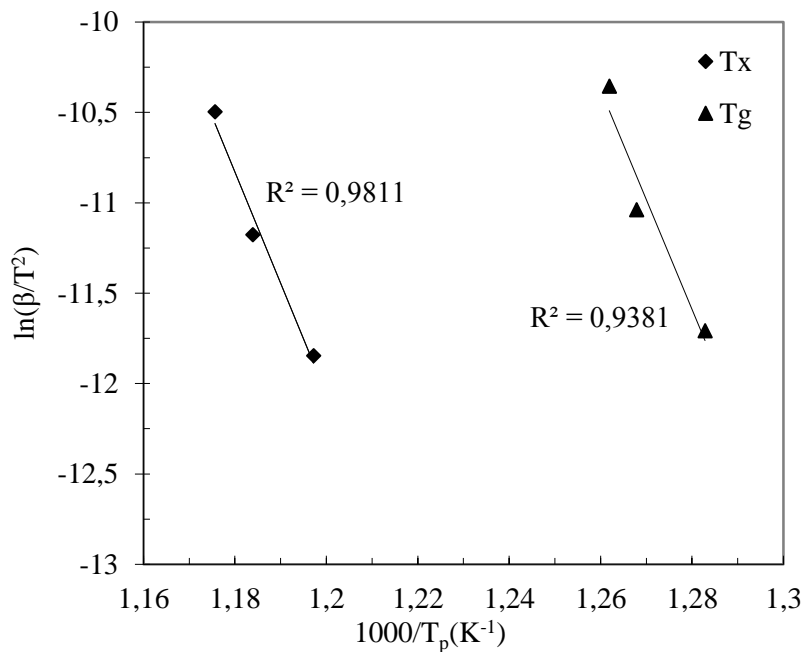
Figure 4.19 Kissinger plot of $Cu_{49}Hf_{42}Al_9$ bulk amorphous alloy

Table 4.5 The activation energies of glass transition and crystallization calculated by using Kissinger method

Transition	Activation Energy(kJ/mol)
Glass transition	438.24
Crystallization	449.54

The activation energy of crystallization indicates the energy barrier which the atoms should overcome to transform from disorder to order states. The higher activation energy values of crystallization present higher thermal stability of amorphous nature of $Cu_{49}Hf_{42}Al_9$ bulk amorphous alloy.

Ozawa [69] and Bosewell methods [70] were applied in order to confirm the results of Kissinger approach. When the three methods were compared, the results were in a positive agreement with each other.
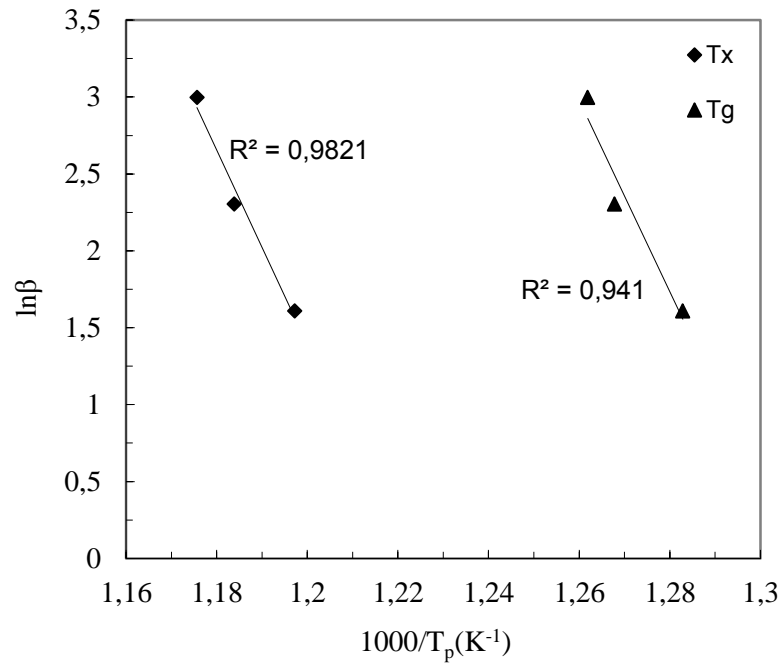
Figure 4.20 Ozawa plot of $Cu_{49}Hf_{42}Al_9$ bulk amorphous alloy

Table 4.6 The activation energies of glass transition and crystallization calculated by using Ozawa method

Transition	Activation Energy(kJ/mol)
Glass transition	436.96
Crystallization	448.09
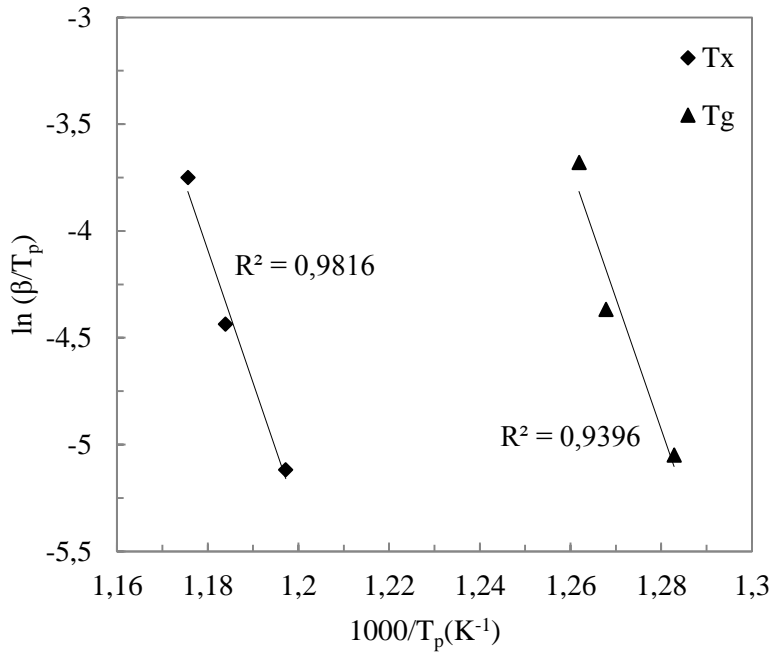
Figure 4.21 Bosewell plot of $Cu_{49}Hf_{42}Al_9$ bulk amorphous alloy

Table 4.7 The activation energies of glass transition and crystallization calculated by using Bosewell method

Transition	Activation Energy(kJ/mol)
Glass transition	437.1
Crystallization	448.74

The critical cooling rate for the eutectic reaction was estimated by using Barandiaran-Colmenero approach [71]. One peak could be seen from each DSC curve since the eutectic reaction was overlapped with the peak of melting event due to less temperature difference between eutectic reaction and melting. Differential scanning calorimetry examinations were done at the scanning rates of 10, 20, 40 °C/min.
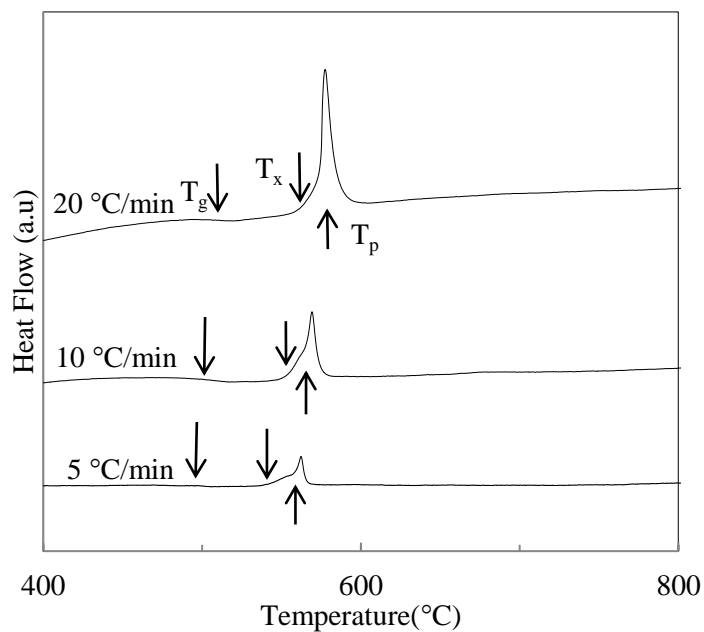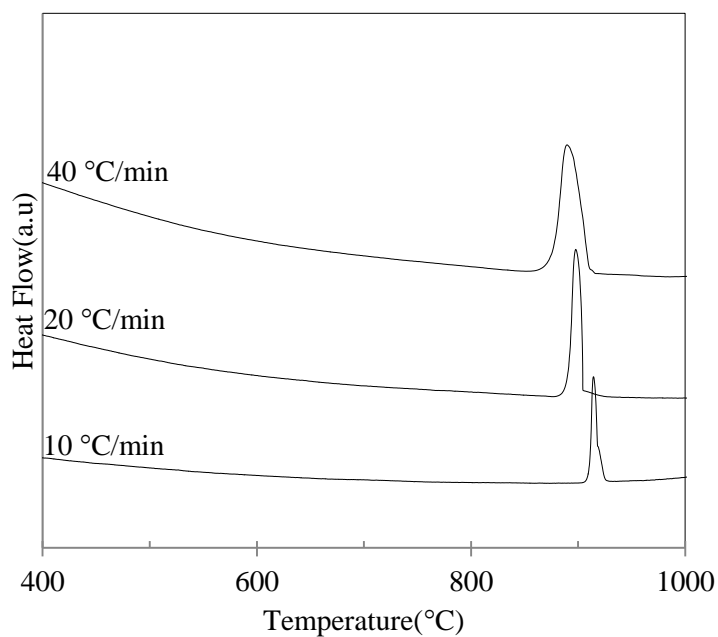
Figure 4.22 DSC thermograms of the scanning rates of 10°C/min, 20°C/min and 40°C/min
(Cooling Curves)

Table 4.8 Thermodynamic Temperatures at the heating rates of
10°C/min, 20 °C/min and 40°C/min

Scanning Rate(°C)	T_l(heating)	T_{xc}(cooling)
10	959.32	919.20
20	964.67	904.87
40	969.88	910.37

The values of Table 4.8 were utilized in order to acquire ln R versus $(T_l - T_{xc})^2$ graph. The graph is illustrated on the Figure 4.23.

43
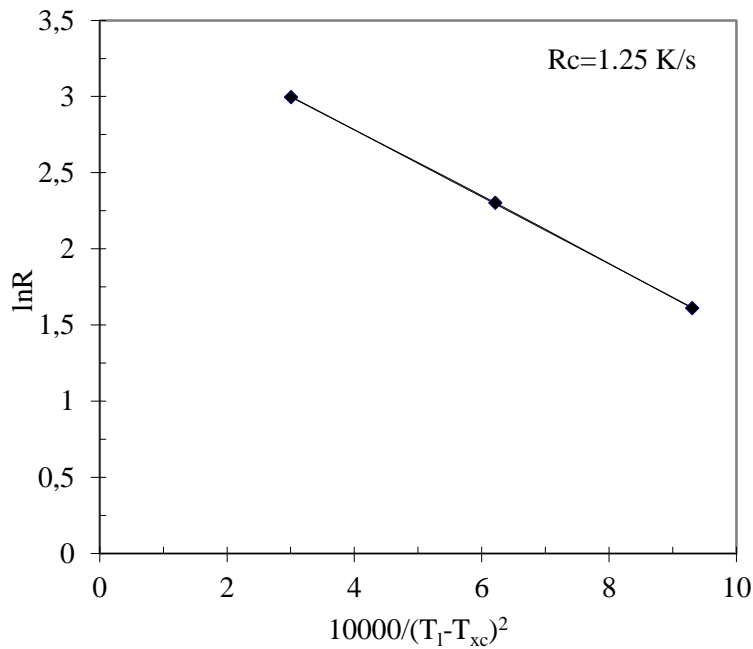
Figure 4.23 The critical cooling rate plot of amorphous $Cu_{49}Hf_{42}Al_9$ alloy

From the slope of the graph, the critical cooling rate for eutectic reaction was found to be 1.25 K/s. This low critical cooling rate value indicates that the $Cu_{49}Hf_{42}Al_9$ alloy is an easy glass forming alloy.

4.3.2 Isothermal Crystallization Kinetics of $Cu_{49}Hf_{42}Al_9$ Alloy

In this part, isothermal crystallization kinetics is discussed. The isothermal crystallization kinetics of $Cu_{49}Hf_{42}Al_9$ alloy was studied by X-ray diffraction, DSC and NanoSEM. Two samples were selected for the examinations. One was analyzed in the supercooled region and the other was examined above the crystallization temperature. The annealing temperatures were 650°C and 540°C and annealing times were 2 and 5 hours. The resultant microstructures are demonstrated on the Figure 4.24. For a better comparison, the microstructure of the amorphous sample is also shown.
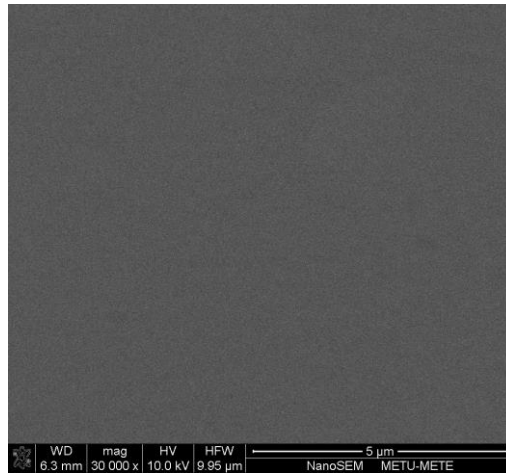
a
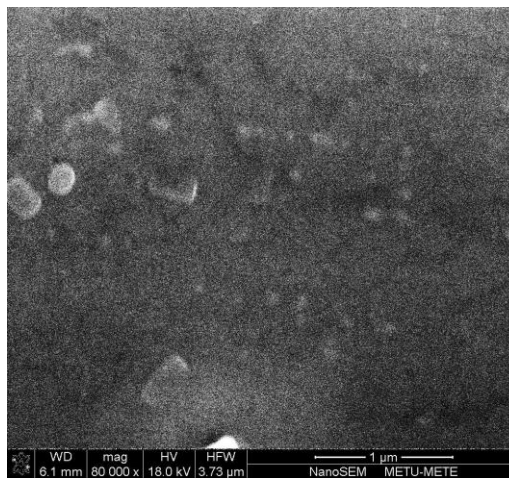
b
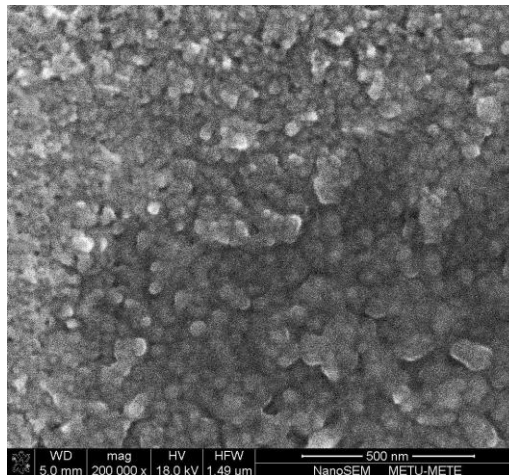
c

Figure 4.24 Backscatter images of a) amorphous sample, b) isothermally heated sample
at 540°C, c) isothermally heated sample at 650°C

In the crystallization process, nanoparticles were precipitated from amorphous matrix. In order to identify the crystalline phase, EDS analysis and XRD were employed. It was difficult to determine the composition of nanocrystalline phase by EDS analysis. XRD pattern is shown on the Figure 4.25 which implied that $CuHf_2$ phase precipitated in nano-scale dimensions from amorphous matrix.
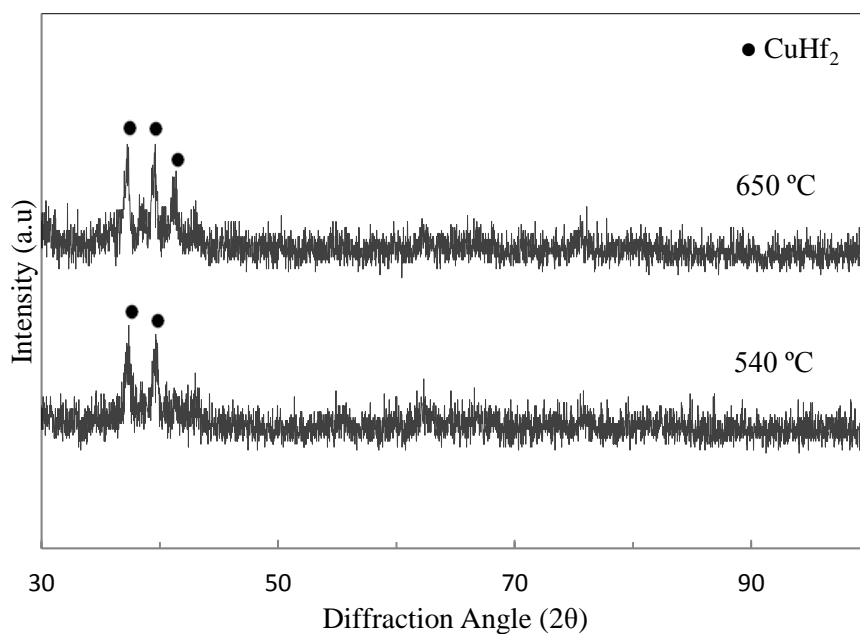
Figure 4.25 XRD pattern of annealed samples

Scherer's formula was applied to determine the particle size. The grain diameter of nanocrystals was estimated to be approximately 20.72 nm.

The kinetics and underlying mechanism for the nucleation and growth of the $CuHf_2$ phase was performed by differential scanning calorimetry studies. The isothermal DSC scans of the samples at 540°C and 650°C are given in the Figure 4.26.

a

b
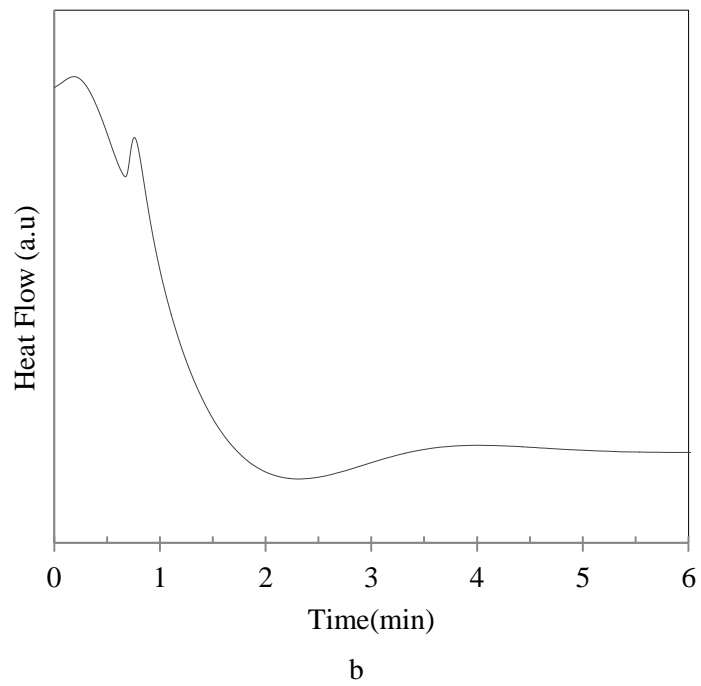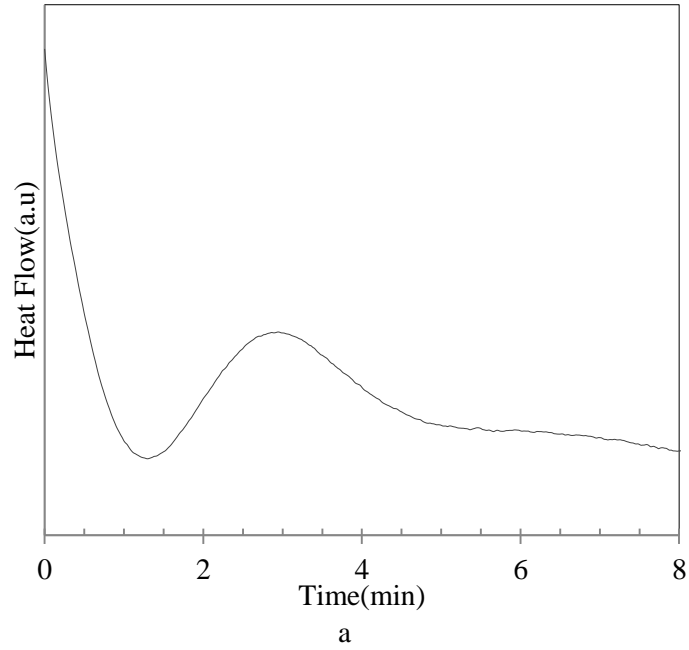
Figure 4.26 Isothermal DSC curves a) at 540°C 5 hour b) 650°C 2 hour

The isothermal crystallization kinetics was analyzed by Johnson-Mehl-Avrami equation 2.14. The crystallized volume fraction (x) was found by measuring the area of the crystallization peak. In order to get detailed information, crystallized volume fraction (x) versus time graph was drawn. The graph is sigmoidal type and exhibited on Figure 4.27.
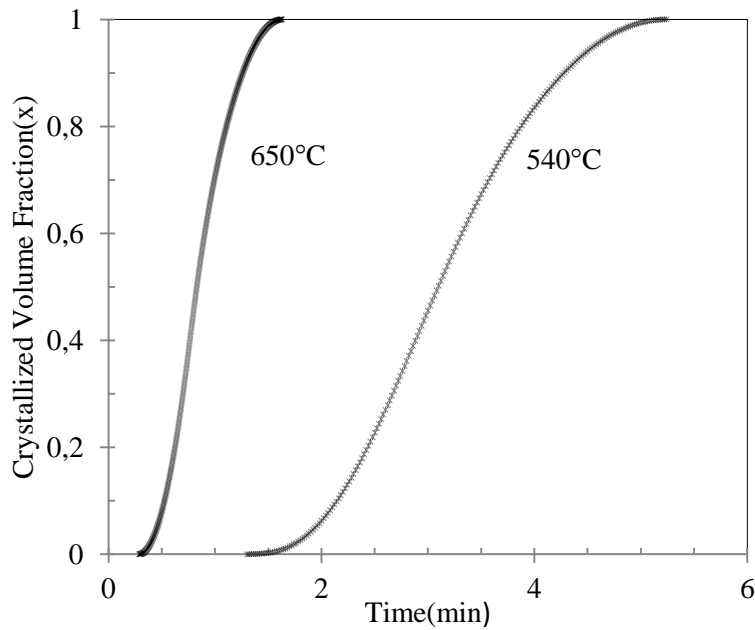
Figure 4.27 The crystallized volume fraction as a function of annealing time

The incubation times (τ) at 650°C and 540°C temperatures were estimated to be 0.29 and 1.3 from the graph. The incubation time is decreased as the annealing temperature is increased due to higher mobility at higher temperatures. The JMA plots at 650°C and 540°C were acquired by plotting ln [ln (1/(1-x)] versus ln(t- τ) as indicated on the Figure 4.28. The values between 0.2≤x≤0.8 give a straight line. Avrami exponenets and the reaction constants were found from the slope and intercept of the lines.
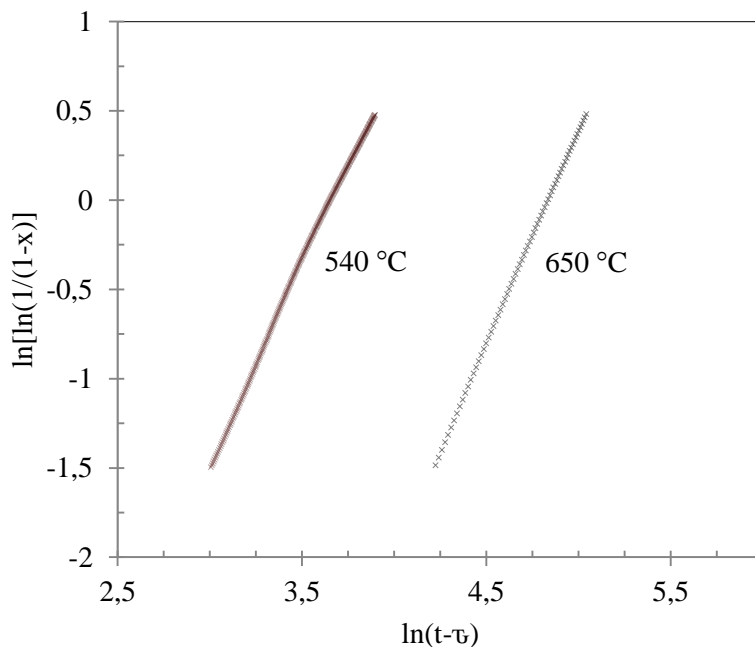
Figure 4.28 Avrami plots of ln [ln (1/(1-x)] versus ln(t-τ) at different temperatures obtained from isothermal DSC scans

Table 4.9 The kinetic parameters of bulk amorphous $Cu_{49}Hf_{42}Al_9$ alloy isothermally annealed at different temperatures

Annealing Temperature(°C)	Incubation Time(min)	Avrami Exponent,n	Reaction Constant,k
540 °C	1.3	2.40	0.008
650°C	0.29	2.23	0.026

The average Avrami exponent value is 2.3 implying that the crystallization process was governed by diffusion controlled three-dimensional growth with decreasing nucleation rate [88].

During the whole crystallization process, the nucleation and growth behavior are not stable. It could be changed at different stages or at different crystallized fractions. For this reason, the variations of local Avrami exponent during crystallization were examined. The local Avrami exponent $n(x)$ [75] was computed by using the Equation 2.12. The results are shown on the local Avrami exponent (n) versus crystallized fraction (%) curve as given on the Figure 4.29.
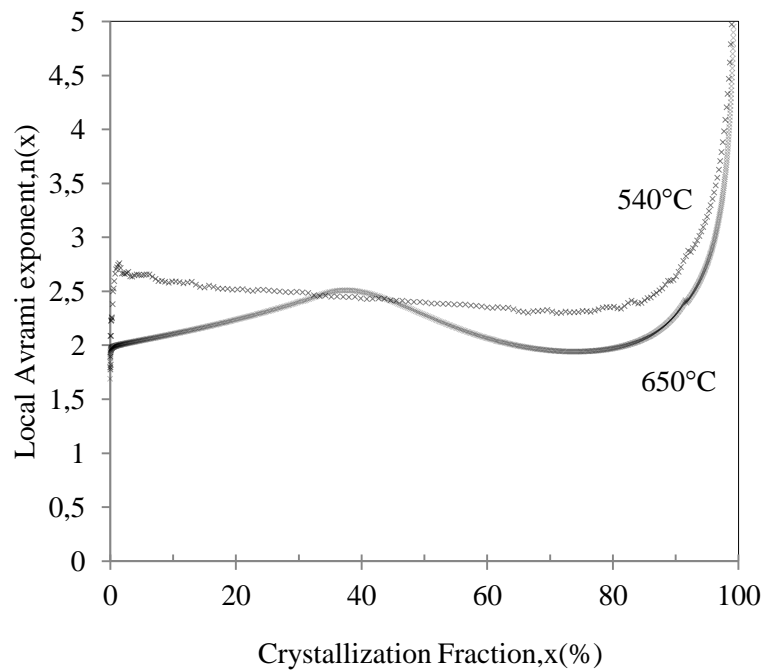
Figure 4.29 Relationship between the local avrami exponent and crystallization fraction at different annealing temperatures

The crystallization process was controlled by one-dimensional growth with decreasing nucleation rate at the beginning stages of crystallization, but the process was mainly governed by diffusion-controlled three-dimensional growth with decreasing nucleation rate at the continuing stages. The evaluations were done between the 0≤crystallization fraction, x(%)≤90 since the Avrami exponent calculations based on J-M-A analysis could result in large uncertainties at the end of crystallization process [77].

CHAPTER 5

CONCLUSIONS

In this study, it is aimed to produce Copper based bulk metallic glass. Following the synthesizing stage, characterization techniques were applied to the samples. The results can be summarized as follows:

1. Amorphous phase formation was not achieved for $Cu_{70}Hf_{30}$ and $Cu_{50}Hf_{50}$ binary alloys under non-equilibrium soldification conditions using water cooled Cu crucible due to poor GFA of these alloys. Therefore, aluminum was chosen as ternary alloying element in order to improve glass forming ability.

2. Aluminum addition to the Cu-Hf system dramatically increased GFA. Hence, bulk amorphous sample with 3 mm diameter was synthesized. Differential scanning calorimetry studies showed that glass forming ability parameters such as T_{rg} and ΔT_x of $Cu_{49}Hf_{42}Al_9$ vitreous alloy are in good agreement with the results reported in the literature.

3. Eutectic reaction was found to exist in the solidification of the alloy under the near equilibrium conditions. However, amorphous phase formation was achieved under non-equilibrium solidifying conditions owing to the suppression of the eutectic reaction. The critical cooling rate for the suppression of the eutectic reaction was found to be 1.25 K/s by isochronal crystallization kinetics indicating that the alloy could be obtained in fully glassy state by applying low cooling rates.

4. The amorphous samples were annealed in the vicinity of T_x which contributed to single stage crystallization of $CuHf_2$ nanocrystals from the amorphous precursor. The average particle size of these nanocrystals was about 20 nm. The activation energy of this crystallization process was estimated to be 449.5 kJ/mol by Kissinger method and the average Avrami exponent value was determined as 2.3 implying that the crystallization process was governed by diffusion controlled three-dimensional growth with decreasing nucleation rate.

REFERENCES

[1] Joysurya Basu and S. Ranganathan, *Bulk metallic glasses: A new class of engineering materials*, Sadhana Vol. 28, Parts 3 & 4, June/August (2003), pp. 783–798.

[2] A. Takeuchi and A. Inoue, *Classification of Bulk Metallic Glasses by Atomic Size Difference, Heat of Mixing and Period of Constituent Elements and Its Application to Characterization of the Main Alloying Element*, Materials Transactions, Vol. 46, 12 (2005), pp. 2817-2829.

[3] N. Mattern, *Structure Formation in Metallic Glasses*, Microstructure Analysis in Materials Science, (2005), pp 1-3.

[4] C.L.Dai, H.Guo, Y. Shen,Y. Li, E.Ma,J.Xu, *A new centimeter diameter Cu based bulk metallic glass*,Scripta Materialia 54 (2006), pp 1403-1408.

[5]Y.C Kim, D.H.Kim, J.C.Lee, *Formation of ductile Cu-based bulk metallic glass matrix composite by Ta addition*, Material Transactions 44 (2003), pp 2224-2227.

[6] Q.Zhang, W.Zhang, A.Inoue, *New Cu-Zr based bulk metallic glasses up to 1.5 cm*, Scripta Materialia 55 (2006), pp 711-713.

[7] W. Zhang and A. Inoue, *Thermal Stability and Mechanical Properties of Cu-Hf-Al Base Bulk Glassy Alloys with a Large Supercooled Liquid Region of Over 100 K*, Materials Transactions,44, (2003) pp. 2346-2349.

[8] W. Klement, R. H. Willens and P. Duwez, *Non-crystalline Structure in Solidified Gold-Silicon Alloys*, Nature, 187 (1960), pp. 869-870.

[9] H.S. Chen, D. Turnbull, *Formation, Stability and Structure of Palladium-Silicon Based Alloy Glasses*, Acta Metallurgica 17 (1969), pp.1021-1031.

[10] H. W. Kui, A. L. Greer and D. Turnbull, *Formation of Bulk Metallic Glass by Fluxing*, Applied Physics Letters, 45 (1984), pp.615-616.

[11] A. Inoue, T. Zhang, T. Masumoto, *Al–La–Ni amorphous alloys with a wide supercooled liquid region*, Materials Transactions, JIM 30 (1989), pp.965–972.

[12] A. Inoue, T. Nakamura, N. Nishiyama and T. Masumoto, *Mg-Cu-Y bulk amorphous alloys with high tensile strength produced by a high-pressure die casting method*, Materials Transactions, JIM, 33 (1992), pp. 937-945.

[13]A. Peker, W. L. Johnson, *A highly processable metallic glass $Zr_{41.2}Ti_{13.8}Cu_{12.5}Ni_{10.0}Be_{22.5}$*, Applied Physics Letters 63 (1993), pp.2342–2244.

[14] J. F Löffler, *Bulk metallic glasses*, Intermetallics 11 (2003), pp.529-540.

[15] A. Inoue , A. Takeuchi,*Recent development and application products of bulk glassy alloys*, Acta Materialia 59 (2011),pp 2243–2267

[16] P.D.Gebenedetti, F.H.Stilinger, *Supercooled Liquids and the glass transition*, Nature Vol 410 (2001), pp 259-267.

[17] W. Kauzmann, *The nature of the glassy state and the behavior of liquids at low temperatures*, Chemical Reviews, 43 (1948), pp.219-256.

[18] D.Turnbull, *Formation of Crystal Nuclei in Liquid Metals,* J.Appl.Phys. 21, (1950),pp 1022-1028.

[19]A.Inoue and K.Hashimoto, *Amorphous and nano-crystalline materials preparation,properties and applications*, Springer Heidelberg Press (2010), pp 1-10

[20]Peker, A (1994), *Formation and characterization of bulk metallic glasses.* Dissertation (Ph.D.), California Institute of Technology

[21] R. Busch, *The* thermophysical properties of bulk metallic glass-forming liquids; JOM 52, (7) (2000), pp 39-42.

[22] M. Heilmaier, J. Eckert, *The Synthesis and Properties of Zr-Based Metallic Glasses and Glass-Matrix Composites*, JOM 52(2000), pp 43-47.

[23] C.A. Angell, *Formation of Glasses from Liquids and Biopolymers,* Science 267 (1995), pp 1924-1935.

[24] R.Busch, W.Liu, W.L.Johnson, *Thermodynamics and kinetics of the $Mg_{65}Cu_{25}Y_{10}$ bulk metallic glass forming liquid,* J. Appl. Phys. 83 (1998),pp 4134-4141.

[25] G. Shao, *Thermodynamic and kinetic aspects of intermetallic amorphous alloys*, Intermetallics, 11 (2003), pp. 313-324.

[26] D. Turnbull, *Under What Conditions Can a Glass be Formed*, ContemporaryPhysics 10 (1969), pp.473-488.

[27] A.Inoue, T.Zhang, T.Masumoto, *Reductilization of embrittled La-Al-Ni amorphous alloys by viscous flow deformation in a supercooled liquid region*, J Non-Crystalline Solids, 156/158, (1993), pp 598−602.

[28] Y.Bing, D. Yong,L Yong,*Recent progress in criterions for glass forming ability*, Trans.Non-Ferrous Met.Soc 19,(2009),pp 78-84.

[29] K. Mondal and B. S. Murty, *On the parameters to assess the glass forming ability of liquids*, Journal of Non-Crystalline Solids, 351 (2005), pp. 1366-1371.

[30] G.J. Fan, H. Choo, P.K. Liaw, *A new criterion for the glass-forming ability of*

liquids,Journal of Non-Crystalline Solids 353 (2007),pp 102–107.

[31] A. Hruby, *Evaluation of glass-forming tendency by means of DTA*, Czechoslovak Journal of Physics, 22 (1972), pp. 1187-1193.

[32] M. V. Akdeniz, A. O. Mekhrabov and M. K. Pehlivanoğlu, *Solidification behaviour of bulk glass-forming alloy systems*, Journal of Alloys andCompounds, 386 (2005), pp.185-191.

[33] R.J Highmore and A.L.Greer: *Eutectics and the formation of amorphous alloys*, Nature 339 (1989), pp 363-365.

[34] L. Zhao,Z.Zheng,J Zhang,S. Dang,C. Ma and T. Zhang, *Composition design and glass-forming ability of Ti-based bulk metallic glasses*,International Journal of Modern physics B,Vol 24,Nos 15,16(2010), pp2326-2331.

[35] X. H. Lin and W. L. Johnson, *Formation of Ti-Zr-Cu-Ni bulk metallic glasses,J.* Appl. Phys. 78 (1995), pp 6514-6519.

[36] H. Choi-Yim,R. Busch, and W. L. Johnson, *The effect of silicon on the glass forming ability of the $Cu_{47}Ti_{34}Zr_{11}Ni_8$ bulk metallic glass forming alloy during processing of composites*, J. Appl. Phys 83(1998), pp 7993-7997.

[37] A.Inoue, W.Zhang, T.Zhang and K.Kurosaka, *Thermal and mechanical properties of Cu-based Cu-Zr-Ti bulk glassy alloys*, Materials Transactions 42 (2001), pp 1149-1151.

[38] A. Inoue, W.Zhang, T. Zhang and K.Kurosaka, *Formation and mechanical properties of Cu–Hf–Ti bulk glassy alloys,* J. Mater. Res.16 (2001), pp 2836-2844.

[39] D. Wang,Y. Lia,B. B. Sun, M. L. Sui,, K. Lu,E. Ma ,*Bulk metallic glass formation in the binary Cu–Zr system*, Appl. Phys Letters 84 (2004),pp 4029-4031.

[40] G. Duan, D. Xu and W. L. Johnson, *High copper content bulk glass formation in bimetallic Cu-Hf system*, Metallurgical and Materials Transactions A 36A (2005), pp 455-458.

[41] P. Jia, H. Guo, Y. Li b, J. Xu and E. Ma , *A new Cu–Hf–Al ternary bulk metallic glass with high glass forming ability and ductility*, Scripta Materialia 54 (2006) pp 2165–2168.

[42] P.Jia and J. Xu, *Comparison of bulk metalli glass formation between Cu-Hf binary and Cu-Hf-Al ternary alloys*, J.Mater.Res. 24 (2009) pp 96-106.

[43] W.Zhang, Q. Zhang, C. Qin and A. Inoue,*Synthesis and properties of Cu–Zr–Ag–Al glassy alloys with high glass-forming ability*, Materials Science and Engineering B 148 (2008),pp 92–96.

[44] C. Suryanarayana, A. Inoue, *Bulk Metallic Glasses*, CRC P. U.S.A., 2011, pp 145-186.

[45] Kui, H.W., A.L. Greer, and D. Turnbull, *Formation of bulk metallic glass by fluxing*.

Appl. Phys. Lett. 45, (1984), 615–616.

[46] Crystal growth techniques, *http://www.innovent-jena.de. /en/INNOVENT_4853*, 2012.

[47] W.Zhang, Q.Zhang, C.Qin and A.Inoue,*Synthesis and properties of Cu–Zr–Ag–Al glassy alloys with high glass-forming ability*, Materials Science and engineering B 148 (2008), pp 92-96.

[48] L.Ma, L.Wang, T.Zhang, *Fabrication of bulk glassy $Hf_{50}Cu_{30}Ni_{10}Al_{10}$ alloy by copper mold casting*, Materials Transactions 43 (2002), pp 2357-2359.

[49] Yam, L. C., *Effect of a minör addition of Si,Sn and In on formation and mechanical properties of Cu-Zr-Al bulk metallic glass*, B.S. Thesis, City University of Hong Kong,2008, 32 p.

[50] Greer, A. L., *Metallic Glasses*, Science, 267, (1995), pp 1947-1953.

[51] Sheng, H. W. Luo, W. K.; Alamgir, F. M.; Bai, J. M.; Ma, E., *Atomic Packing and Short-to-Medium-Range Order in Metallic Glasses*, Nature 439,(2006),pp 419-425.

[52] A. R Yavari, J. J Lewandowski, J Eckert, *Mechanical Properties of Bulk Metallic Glasses*, MRS Bulletin,32, (2007)**,** pp635-638.

[53] M. Stoica,, J. Eckert, S. Roth, Z.F. Zhang, L. Schultz, W.H. Wang,*Mechanical behavior of $Fe_{65.5}Cr_4Mo_4Ga_4P_{12}C_5B_{5.5}$ bulk metallic glass, Intermetallics*, 13 (2005) ,pp 764–769

[54] F. Jiang, Z.B. Zhang, L. He and J. Sun, *The effect of primary crystallizing phases on mechanical properties of $Cu_{46}Zr_{47}Al_7$ bulk metallic glass composites*. Mater. Res. 21 (2006), pp. 2638-2645.

[55] A.Inoue and A.Takeuchi, *Recent progress in bulk glassy alloys*, Materials Transactions 43 (2002), pp 1892-1906.

[56] A. Inoue, A. Murakami, T. Zhang and A. Takeuchi, *Thermal stability and magnetic properties of bulk amorphous Fe-Al-Ga-P-C-B-Si alloys*, Materials Transactions JIM 38 (1997), pp 189-196.

[57] B.L. Shen, A. Inoue, *Bulk Glassy Fe-Ga-P-C-B-Si Alloys with High Glass forming Ability, High Saturation Magnetization and Good Soft Magnetic Properties*Mater. Trans. 43 (2002) pp 1235-1239.

[58] M. Aykol, M. V.Akdeniz and A. O. Mekhrabov,*Solidification behavior, glass forming ability and thermal characteristics of soft magnetic Fe-Co-B-Si-Nb-Cu bulk amorphous alloys*, Intermetallics 19 (2011), pp 1330-1337.

[59] K.Asami, C.-L.Qin, T.Zhang, and A.Inoue, *Effect of additional elements on the corrosion behaviour of a Cu-Zr-Ti bulk metallic glass*, Mater.Sci.Eng.A 375-377, (2004), pp 235-239.

[60] B.Liu and L.Liu, *The effect of microalloying on thermal stability and corrosion resistance of Cu-based bulk metallic glasses*, Mater.Sci.Eng.A 415(1-2), (2006), pp 286-290.

[61] C. L. Qin, K. Asami, T. Zhang, W. Zhang, and A. Inoue, *Corrosion behavior of Cu–Zr– Ti–Nb bulk glassy alloys*, Mater. Trans. 44(4), (2003), pp 749–753.

[62] C. L. Qin, W. Zhang, K. Asami, N. Ohtsu, and A. Inoue, *Glass formation, corrosion behavior and mechanical properties of bulk glassy Cu–Hf–Ti–Nb alloys*, Acta Mater.53(14), (2005),pp 3903–3911

[63] L. Liu and B. Liu, *Influence of the micro-addition of Mo on glass forming ability and corrosion resistance of Cu-based bulk metallic glasses*, Electrochim. Acta 51(18), 2006, pp 3724– 3730.

[64] C. L. Qin, W. Zhang, H. Kimura, K. Asami, and A. Inoue, *New Cu–Zr–Al–Nb bulk glassy alloys with high corrosion resistance*, Mater. Trans. 45(6), (2004), pp 1958–1961.

[65] B. Liu, L. Liu, M. Sun, C. L. Qiu, and Q. Chen, *Influence of Cr micro-addition on the glass forming ability and corrosion resistance of Cu-based bulk metallic glasses*, ActaMetall. Sin.41 (7), (2005), pp 738–742.

[66] C. L. Qin, K. Asami, T. Zhang, W. Zhang, and A. Inoue, *Effects of additional elements on the glass formation and corrosion behavior of bulk glassy Cu–Hf–Ti alloys*, Mater.Trans. 44(5), (2003), pp 1042–1045.

[67] H.E. Kissinger, *Reaction Kinetics in Differential Thermal Analysis*, Analytical Chemistry, 29 (1957), pp.1702-1706.

[68] Y.J. Yang, D.W. Xing, J. Shen, J.F. Sun, S.D. Wei, H.J. He and D.G. McCartney, *Crystallization kinetics of a bulk amorphous Cu–Ti–Zr–Ni alloy investigated by differential scanning calorimetry*, Journal of Alloys and Compounds 415 (2006), pp 106–110.

[69] T. Ozawa, *A new method of analyzing thermogravimetric data,* Bulletin Chemical Society of Japan, 38 (1965), pp.1881-1886.

[70] P.G. Boswell, *On the calculation of activation energies using a modified Kissinger method*, J. Thermal Analysis 18 (1980), pp 353-358.

[71] JM Barandirán, J. Colmenero, *Continuous cooling approximation for the formation of a glass,* Journal of Non-Crystalline Solids 46(3) (1981), pp 277‑287.

[72] E. J Mittemeijer, *Analysis of the kinetics of phase transformations*, Journal of Materials Science, 27 (1992), pp 3977−3987.

[73] A.Calka, A.P Radlinski, *Decoupled bulk and surface crystallization in Pd85Si15 glassy metallic alloys: Description of isothermal crystallization by a local value of the*

Avrami exponent, Journal of Materials Research 3 (1988), pp 59−66.

[74] M.Avrami*, Kinetics of phase changeI General theory*, The Journal of Chemical Physics 7 (1939), pp 1103−1112.

[75] J.W. Christian, *The theory of transformation in metals and alloys*, New York Pergamon Press Inc, (1975), pp 542−550.

[76] K. H. Buschow, *Stability and electrical transport properties of amorphous $Ti_{1-x}Ni_x$ alloys*, Journal of Physics F−Metal Physics 13 (1983), pp 563−572.

[77] L. Liu, Z.F. Wu, J. Zhang, *Crystallization kinetics of $Zr_{55}Cu_{30}Al_{10}Ni_5$ bulk amorphous alloy*, Journal of Alloys and Compounds 339 (2002), pp 90–95.

[78] K.F. Kelton, T.K. Croat, A.K. Gangopadhyay, L.-Q. Xing , A.L. Greer ,M. Weyland , X. Li and K. Rajan,*Mechanisms for nanocrystal formation in metallic glasses*,Journal of Non-Crystalline Solids 317 (2003),pp 71–77.

[79] T.Kulik, T.Horubala, H.Matyja, *Flashannealing nanocrystallization of Fe-Si-B based glasses*, Mater.Sci.Eng.A 157 (1992), pp 107-113.

[80] T.Kulik, D.Bucka, H.Matyja, *Effect of flash annealing on the grain size and morphologyof crystallization products of Co-Si-B glasses*, Mater. Sci. Lett. 12 (1993), pp 76-79.,

[81] T.Kulik, J.Ferenc, H.Matyja, *Low temperature nanocrystallization iron based amorphous alloys*, Materials Science Forum 235-238 (1997), pp 421-426.

[82] U.Köster and J. Meinhardt*, Crystallization of Highly Undercooled Metallic Melts and Metallic Glasses Around the Glass Transition Temperature*, Mater. Sci. Eng. A178 (1994), pp 271-278.

[83] Y.L Gao, J. Shen, J.F Sun, D.M. Chen, G. Wang, H.R Wang, D.W Xing, H.Z Xian, B.D Zhou, *Nanocrystallization of Zr–Ti–Cu–Ni–Be bulk metallic glass*, Materials Letters 57 (2003), pp 2341– 2347.

[84] T.Kulik*, Nanocrystallization of metallic glasses*, Journal of Non-Crystalline Solids 287 (2001), pp 145-161.

[85] C.L Yang, G.C Yang, Y.P Lu, Y.Z Chen and Y.H.Zhou, *Phase selection in highly undercooled Fe-B eutectic alloy melts*,Trans. Nonferrrous Met.Soc. 16 (2006), pp 39-43.

[86] D.M. Herlach, *Non-equilibrium solidification of undercooled metallic melts*, Mater Sci Eng R 12 (1994), pp 252-272.

[87] P.R Subramanian and D.E Laughlin, *The Cu-Hf system*, Bulletin of Alloy Phase Diagrams 9(1) (1988), pp 51-55.

[88] J. W. Christian, *The theory of transformation in metals and alloys*, Oxford Pergamon Press Inc, (1965), pp 489−500.